Use of Lasers in Medicine: Tissue Soldering and Precise Cutting

Diplomarbeit

der Philosophisch-naturwissenschaftlichen Fakultät
der Universität Bern

vorgelegt von

David Haberthür

2002

Leiter der Arbeit:

Prof. Dr. Martin Frenz

Biomedizinische Photonik
Institut für angewandte Physik

Abstract

Use of Lasers in Medicine:

Tissue Soldering and Precise Cutting

The present master thesis addresses two topics in lasers in medicine.

Chapter 1 gives a short introduction into the field of the use of lasers in medicine, with emphasis on the basics of light propagation in tissue.

Chapter 2 discusses the possibilities and problems of using an infrared diode-laser to coagulate a dye-enhanced solder to join cartilage tissue. Up to now only a few research groups have attempted to solder cartilage by using a laser. Articular cartilage is a complex tissue, that once damaged, has little capacity for permanent repair. The goal of the study was to evaluate the influence of laser parameters and solder ingredients on the tensile strength and the thermally induced cartilage damage of a bond between cartilage and an implant. The implant consisted either of native articular cartilage or of artificial cartilage made of collagen fibers.

Chapter 3 finally focusses on the use of a pulsed Er:YAG (erbium doped yttrium aluminum garnet) laser for ablation and cutting of calcified tissue. Removal of calcified tissue, especially aortic valve replacement is generally accomplished by a major surgical procedure. To lessen the costs and to

reduce the implications such a major surgery has on the patient, an endovascular procedure for valve replacement provides an alternative to open heart surgery. The presented work was intended to evaluate the feasibility of cutting calcified heart valves with an Er:YAG laser in view of an endovascular procedure.

Contents

Abstract **iii**

1 Introduction **1**
1.1 Motivation and Overview 1
1.2 Light Propagation in Biological Tissue 3
1.2.1 Scattering 4
1.2.2 Absorption 5

2 Cartilage Soldering **7**
2.1 Introduction and Overview 7
2.1.1 Background 7
2.1.2 Cartilage Damage 8
2.1.3 Laser Assisted Cartilage Soldering 11
2.2 Material and Methods 13
2.2.1 Laser Source and Light Delivery System 13
2.2.2 Cartilage Samples 15
2.2.3 Artificial Cartilage – Collagen Matrices 17
2.2.4 Solder 19
2.2.5 Soldering Procedure 22
2.2.6 Tensile Strength Evaluation 24
2.2.7 Tissue Viability – Live/Dead-Staining 24
2.3 Monte-Carlo-Simulation 27
2.4 Results 33
2.4.1 Influence of Solder Ingredients on Tensile Strength . . . 33
2.4.2 Matrices 35
2.4.3 Thermally Induced Tissue Damage 37
2.5 Discussion 40
2.5.1 Monte-Carlo-Simulation and Tensile Strength 40
2.5.2 Thermally Induced Tissue Damage 42
2.6 Conclusions 45
2.7 Outlook 46

3 Laser-assisted Ablation of Calcified Tissue **49**
3.1 Introduction and Overview 49
3.1.1 Background 49
3.1.2 Percutaneous Aortic Valve Ablation Using a Laser Device 51
3.1.3 Photoablation of Biological Tissue 53
3.2 Material and Methods 54
3.2.1 Laser Source 54
3.2.2 Light Delivery System 55
3.2.3 Heart Valve Samples and Ablation Process 57
3.3 Results and Discussion 58
3.3.1 Laser and Laser Light Delivery System 58
3.3.2 Ablation 59
3.3.3 Remnant Analysis 61
3.3.4 Tissue Damage 62
3.4 Conclusions 67

Bibliography **72**

List of Figures **74**

List of Tables **75**

Acknowledgements **77**

Chapter 1

Introduction

1.1 Motivation and Overview

Soon after the first laser was running in the early sixties, multiple laser applications were discovered in medicine, and a new research field called laser medicine was born.

In a large number of therapeutic and diagnostic medical applications various laser systems became an extremely useful standard tool. Alone in the domain of tissue soldering and ablation, where the present work is situated, one is able to find a broad range of applications, for example the vascular end-to-end anastomosis [1], nerve repair [2], and soldering of tissue [3, 4]. Other applications are in ophthalmology (e.g. LASIK, PRK[1]) and in various dental applications (e.g. ablation of dentin, treatment of hypersensitive teeth, surface decontamination in Periimplantitis[2] and Periodontitis[3]).

[1] Laser-Assisted in situ Keratomileusis and Photorefractive Keratectomy, both laser assisted vision correction methods.

[2] *Periimplantitis* – Inflammation of the structures around a strained jaw-bone implant which can lead to a deprivation of the surrounding bone material.

[3] *Periodontitis* – Infection and loss of bone from around the teeth. Periodontal disease starts as the swelling of the gum around the teeth, and left untreated can cause the teeth to drift apart and eventually become so loose that they need to be extracted.

Many of the aforementioned applications are clinically approved and widely used, others are still topics of research activities. The laser is however also a powerful tool for diagnostics; it can be used to probe our body for informations about the presence of tumors, or to examine human physiology (e.g. blood flow) non-invasively with pulsed optoacoustic spectroscopy [5] or optical coherence tomography (OCT) [6, 7].

Today, a large number of laser systems cover the electromagnetic spectrum from the far ultraviolet (UV) to the far infrared (IR) providing the user with a possibility to choose from continuous wave (cw), pulsed or ultrashort pulsed modes. The evaluation of the optimal laser system is determined by the desired clinical outcome and the optical properties of the tissue to be treated. The interaction processes depend on the irradiation time, the irradiance and the optical tissue properties. Irradiation time and irradiance can be varied over several orders of magnitude leading to completely different tissue reactions. A low irradiance combined with a long irradiation time characterizes photochemical effects (e.g. biostimulation or photodynamical therapy). Shorter irradiation times and higher irradiances cause thermal effects (e.g. coagulation, evaporation and ablation). Plasma formation leading to mechanical tissue disruption is achieved with the highest irradiances ($> 10^{10}$ W/cm^2) and ultrashort pulses.

A prerequisite for optimal use of lasers in medicine is a fundamental knowledge of the physical phenomena underlying the light propagation in tissue.

1.2 Light Propagation in Biological Tissue

Optical tissue properties determine how laser light interacts with biological tissue. Light irradiated on a target material is reflected, absorbed or scattered and – if the sample is optically thin – even transmitted. The strength of the individual effect essentially depends on the wavelength λ of the incident light, the index of refraction and the attenuation and scattering coefficients μ_a and μ_s of the tissue. In the UV, the main absorbers in tissue are proteins and nucleic acids. In the visible electromagnetic spectrum, the most important absorbers for biological tissue are melanin in the skin and hemoglobin in the blood, whereas in the near and mid infrared water absorption becomes dominant. The highest water absorption is found at λ=3 μm, the wavelength of an Er:YAG laser, caused by fundamental symmetric and asymmetric vibrational stretching and bending modes of the bonds between oxygen and hydrogen in the water molecules. In contrast, scattering continuously decreases from UV towards the infrared.

The soldering and ablation processes in the present work were all heat induced. The heat induced through absorption in the solder or tissue allows – depending on the energy applied – either bonding of tissue without sutures and without contact to the tissue or ablation of tissue with high precision.

To be able to calculate the light distribution in biological tissue – which can be achieved for example by Monte-Carlo-methods – the optical parameters of the tissue have former to be experimentally determined. The Monte-Carlo-method provides a statistical approach towards generating exact solutions to light transport in tissue.

1.2.1 Scattering

Heterogeneities and/or fluctuations in the refractive index of the tissue cause scattering of light. Such inhomogeneities are found from the nanometer scale in macromolecular structures or membranes up to the micrometer scale in cells and extracellular constituents such as collagen fibers. Structures on the scale of the wavelength are the strongest scatterers of visible and near infrared light and yield to a very forward directed scattering. In contrast structures which are much smaller than the wavelength are individually less strong scatterers with in average isotropic scattering. Scattering is not only wavelength dependent, it also varies from type to type of irradiated tissue.

The scattering intensity I in a tissue does scale according to the following formulas [8].

$$I \sim \frac{1}{\lambda^4} \qquad \text{(Rayleigh-Scattering)} \tag{1.1}$$

$$I \sim \frac{1}{\lambda^{0.4-0.5}} \qquad \text{(Mie-Scattering)} \tag{1.2}$$

Rayleigh-Scattering is isotropic and valid if the particles are much smaller than the used wavelength λ, which is the case for macromolecular structures (smaller than 10 nm) or membranes (approximately 100 nm). The intensity in Rayleigh-Scattering does scale with $1+\cos^2\Theta$ (where Θ is the scattering angle), hence the scattering at right angles is half the forward intensity. Formula 1.2 is valid when the particles are much bigger than λ. Our scattering particles have an approximate size of 100–3000 nm in the case of collagen fibers and bigger than 5 μm when single cells are considered as scattering particles. The intensity in Mie-Scattering is scaled mostly in forward direction.

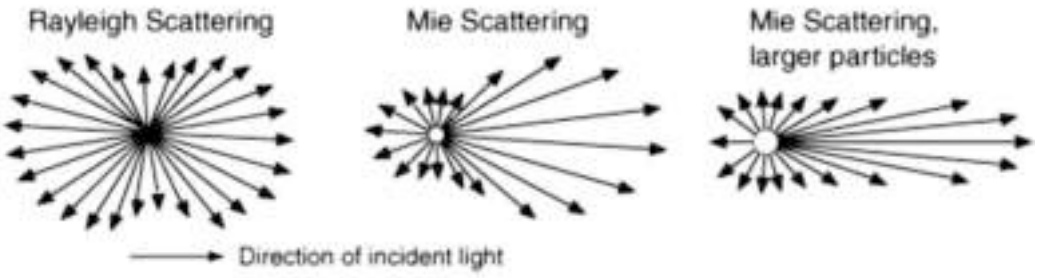

Figure 1.1: Scattering pattern of Rayleigh- and Mie-Scattering.

1.2.2 Absorption

In the case of absorption, the radiation is attenuated according to Beers law (see formulas below) and converted into heat. $I(z)$ is the intensity in Watts per square centimeter in the tissue after the pathlength z, I_0 the incident intensity, μ_a and μ_s are the absorption and scattering coefficients, μ_t is the total absorption coefficient and δ is the optical penetration depth.

$$I(z) = I_0 e^{-(\mu_t)z} \tag{1.3}$$

$$\mu_t = \mu_a + \mu_s \tag{1.4}$$

$$\delta = \frac{1}{\mu_t} \tag{1.5}$$

Thermally induced bonding of tissue is possible in different ways. The tissue to be joined can directly be irradiated whereby the heat is generated in the tissue itself through absorption. Presuming that the laser parameters are adapted, the generated heat provokes coagulation and/or cross linking of tissue collagen therefore bonding the tissue with no intermittent agent. A second possibility is the application of a dye-enhanced solder which selectively absorbs the laser radiation. Preferably the dye is chosen in such a way that the laser radiation is exclusively absorbed in the solder, and mainly transmitted through the cartilage tissue. The bonding of the tissue is achieved

through coagulation of the proteins in the solder which then form the bond between cartilage and solder.

The advantage of this approach in contrast to direct heating of the tissue is that the heat is locally generated in the solder and diffuses from there into the adjacent tissue, which keeps lateral tissue damage minimal. Another advantage of this process is that the outcome of the soldering procedure can exactly be controlled by the irradiated wavelength and absorption coefficient of the solder.

Chapter 2

Cartilage Soldering

2.1 Introduction and Overview

2.1.1 Background

Cartilage is a tough and slippery material with little or no blood circulation, which leads to a slow regeneration after an injury and a low capacity for repair. The weight-bearing, load distributing and lubricating cartilage is a macromelecular tissue composed of around 65 to 85 % water, 10 to 25 % collagen fibers and around 5 to 10 % proteoglycan aggregates. Besides water cartilage tissue has a relatively simple structure, consisting merely of chondrocytes and intercellular matrix substance which absorb the mechanical load. Cartilage usually possesses no nerve fibers, blood vessels or lymphatic system. Chondrocytes are cartilage cells that are involved in buildup and degradation of proteoglycans and collagen. In other words, they are responsible for the synthesis, maintenance, and regeneration of cartilage. Proteoglycans (PGs), along with collagen type II and chondrocyte cells, make up the major part of cartilage and contain sulfur chains. The sulfur gives them

a negative charge which attracts water. This causes PGs to have a gel-like consistency with the ability to fill a space in three dimensions and to absorb and withstand pressure. Intermediary collagen fibers interwoven with the PGs account for the tensile strength in tissue. If PGs are not synthesized, then normal cartilage function is impaired and breakdown is accelerated.

Most cartilage present in mammalian organisms is of the so-called hyaline type, deriving from its glass-like or nearly transparent appearance in native state[1]. The cellular and matrix components of the cartilage generally constitute about 10 and 90 % of the tissue volume, respectively [9]. The extracellular matrix is composed of water, proteoglycans and collagen. The relationship between these components is responsible for the biomechanical properties of the cartilage (for example the weight bearing capacity of multiple hundred kilograms per square centimeter in the human knee).

A smaller part of cartilage tissue includes fibrous cartilage in intervertebral discs, menisci and also in repaired cartilage after an injury and elastic cartilage in the ear and nose. Its combined properties of stiffness and elasticity provide cartilage tissue with the potential to absorb externally applied compressive, tensional and shearing forces [10].

2.1.2 Cartilage Damage

Cartilage tissue damage and injury is a problem in an increasing number of people, especially sporty people. Partial-thickness defects in the articular cartilage do not heal spontaneously, and usually progress until degeneration of the articular surface. This is because surface defects have to rely on sparsely populated chondrocytes for remodelling the extracellular matrix, where deeper lesions of the cartilage may introduce a blood supply from the

[1] *hyalos* – Greek for glass

well vascularized subchondral bone. Injuries that penetrate the subchondral bone undergo repair through the formation of fibrocartilage, instead of the normal hyaline cartilage. From the biomechanical point of view, the problem is that the fibrous cartilage is made to resist tensional forces (e.g. menisci), while the hyaline cartilage is made to resist compression forces (e.g. articular joint surface), to enable smooth articulation, and to withstand long-term variable cyclic load and shearing forces.

In selecting methods of restoring a damaged articular surface, it is important to distinguish between articular cartilage repair and articular cartilage regeneration.

- Repair refers to the healing and restoration of an injured chondral[2] surface or replacement of lost cartilage with new tissue that resembles but does not duplicate the structure, composition, function and durability of articular cartilage. Unfortunately, the repaired articular cartilage generally fails to replicate the attributes of normal hyaline articular cartilage.

- Regeneration refers to the formation of an entirely new articulating surface that is indistinguishable from normal, original hyaline articular cartilage, a process which is still beyond all current surgical techniques. Normal hyaline articular cartilage has never been successfully, reliably reproduced by any technique to date.

Smaller superficial injuries can be treated by debridement of the damaged area using mechanical shavers or laser. Lasers provide a flat joint surface and reduce pain for the patient. Up to now orthopedic surgery does not offer satisfying repair solutions over long terms. Numerous sur-

[2] *chondral* – Composed of cartilage

gical approaches penetrate down to the subchondral bone to stimulate the bone marrow (e.g. subchondral drilling, microfracturing or abrasive arthroplasty[3]). Once disruption of the vascularized bone has occurred, a fibrin clot is formed and cells are introduced into the area. These cells produce a fibroblastic tissue that on an initial biopsy can have a hyaline-like quality and appearance, but degrades over time. The processes involving penetration of the bone offer short- to moderate-term symptom relief, but they all promote the development of fibrous cartilage which lacks the mechanical properties of hyaline cartilage. Larger injuries need the total replacement of the injured area. The high water content of up to 80 % complicates the transplantation process.

A possible answer to this problem is the replacement of the damaged tissue with healthy tissue instead of trying to regenerate the damaged cartilage. Up to now the state of the art technique for a replacement is the Mosaicplasty or Osteochondral Autograft Transplantation (OAT) [11]. In this surgical technique the damaged part of the cartilage is replaced with a healthy piece of cartilage from another part of the joint. For this the surgeon extracts a cylinder of cartilage tissue with a part of the underlying bone. This healthy cartilage graft from an intact part of the joint is then switched with a cylinder of the same size from the damaged part in the joint. The bone at the bottom of these cylinders ensures the attachment and good fit of the grafts in the joint. It further enables the healing of the defect in the joint through providing the blood supply to the cartilage on top of the cylindrical graft and connection to the surrounding bone.

Even so the bone cylinder provides for a good fixation of the implant in the operation site, the integration of the graft into the surrounding cartilage is

[3] *Arthroplasty* – surgical reconstruction or replacement of a malformed or degenerated joint

imperfect. The cartilage implant does not heal nor grow back normally. This is often responsible for a failure of the surgery and can lead to subsequent problems for the patient. Therefore it would be advantageous if the defect can be repaired without the underlying bone and generally it would be preferable to achieve a better cartilage to cartilage connection.

2.1.3 Laser Assisted Cartilage Soldering

In the present work a variant of Mosaicplasty was applied. The main difference compared to OAT is that cartilage tissue was transplanted in a cartilage defect with the use of a solder and without the use of an underlying piece of subchondral bone.

Methods of repairing articular cartilage lesions with lasers are not new in orthopedics, but a breakthrough in long-term restoration on weight-bearing cartilage has still to be shown. Up to now only a few research groups have attempted to bond cartilage using the laser [3, 12]. Despite of numerous attempts by researchers and physicians involved in the field of articular cartilage repair, satisfactory integration or regeneration of hyaline cartilage could not be demonstrated unequivocally.

The strong bond between the replaced and the underlying cartilage without the use of subchondral bone can be achieved by soldering of the implant into the defect. In this study we investigated the feasibility of laser-assisted cartilage soldering using an Indocyanine Green enhanced solder.

Laser assisted tissue repair mediated with an albumin protein solder relies on photothermal bonding induced by light absorption in the solder which is applied to the tissue. The extent of denaturation in the solder is governed by the laser irradiation parameters that determine the heat deposition in the solder and heat diffusion into the adjacent tissue. The refractive index

mismatch at the cartilage-solder interface determines whether photons are reflected or transmitted into the solder. Scattering at the solder surface and within the solder strongly influences the distribution of light within the solder, whereas the conversion of laser light to thermal energy in the solder (and also in the cartilage) depends on the absorption coefficient μ_a. Heat transfer in the tissue depends on the thermal conductivity and thermal diffusivity of the solder and cartilage.

In addition, we investigated the possibilities of replacing the cartilage implants with specially treated collagen matrices. The final goal is to dope these matrices with growth-stimulation substances to encourage healing of the lesion and regrowth of the cartilage tissue into the defect. This would then help to counteract the thermal damage of the cartilage tissue induced through the irradiation and heating of the solder.

The soldering of tissue using an ICG enhanced albumin solder seems to have multiple advantages to Mosaicplasty. The replacement of damaged cartilage tissue can be accomplished without any damage to the underlying bone. The laser assisted cartilage soldering should – in future – allow to replace and repair damaged cartilage of any desired shape.

To characterize the quality of the soldered cartilage-cartilage- or cartilage-collagenmatrix-compound, tensile strength measurements have been carried out.

In addition, the influence of solder composition on the final strength was determined.

The laser-induced thermal damage was assessed with a cell viability test which offered full insight in thermal cell damage induced by the soldering process and mechanical damage to the chondrocytes induced by cartilage preparation. All experiments were accomplished in an in vitro model.

2.2 Material and Methods

2.2.1 Laser Source and Light Delivery System

For all soldering experiments we used a GaAlAs-diode laser system (DL50 from FISBA Optik, St. Gallen, Switzerland) which emits up to 60 W of near infrared radiation at 808 nm. For the experiments we used an irradiation power between 0.5 W and approximately 2.5 W.

The power of the laser beam was measured and recorded with an energy meter (PowerMAX 500D, Molectron with Detector PowerMAX Probe PM30V1, Molectron, Portland, USA).

For the first part of the experiments the light was coupled into a quartz fiber with 600 μm core diameter. The fiber was hand-guided in a helical motion at a distance between 3 to 5 mm above the tissue surface (see figure 2.1). It has to be mentioned that the total amount of energy applied in the process varies from place to place and depends on the speed of movement of the tip.

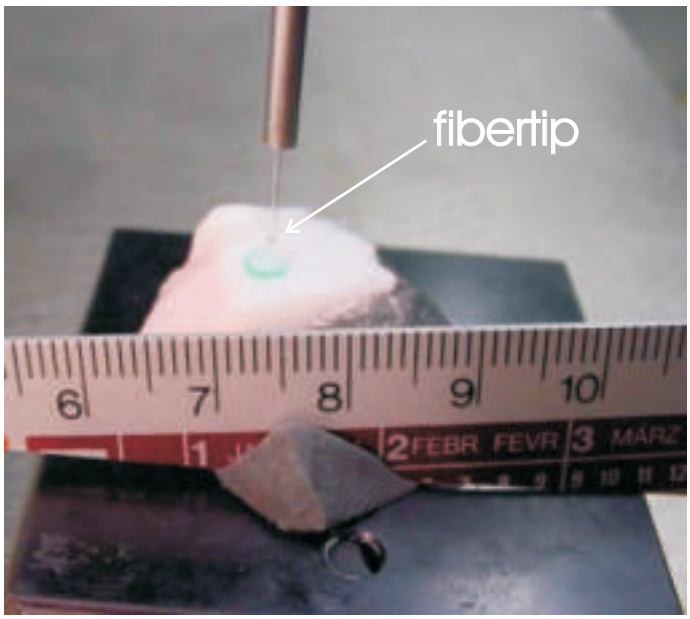

Figure 2.1: Fiber tip on sample during experiment.

Using the formulas below the spot diameter $2R$ on the tissue surface can be calculated. NA is the numerical aperture, Θ is the accepting angle of the fiber, n_1 and n_2 are the refracting indices of the core and cladding, respectively, h is the distance of the fiber to the sample and r is the radius of the core of the fiber (see also figure 2.2).

$$\text{NA} = \sin\Theta = \sqrt{n_1^2 - n_2^2} \tag{2.1}$$

$$\tan\Theta = \frac{R}{h} \tag{2.2}$$

$$R = h\tan(\arcsin(NA)) + r \tag{2.3}$$

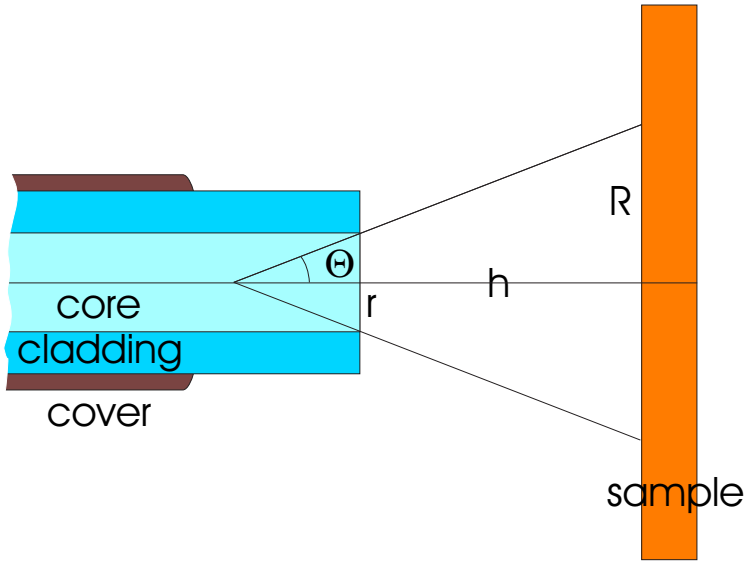

Figure 2.2: Diagram of fiber and spot size on sample.

The calculated spot diameter for a fiber with a NA=0.2 was between 1.82 mm at a distance h of 3 mm and 2.8 mm at h=5 mm, resulting in an irradiance varying from 8.1 W/cm^2 for a low energy and large diameter (0.5 W, 2.8 mm) to 76.9 W/cm^2 for a high energy and small diameter (2 W, 1.8 mm).

To be able to uniformly irradiate the total cartilage implant, we projected the distal fiber tip onto the cartilage surface resulting in a spot diameter slightly bigger than the diameter of the implant. The irradiances used in this second part of the experiments ranged from 1.8 W/cm^2 (6 mm diameter, 0.5 W laser power) up to approximately 9 W/cm^2 (6 mm, 2.5 W). The laser power was not raised, because we wanted to achieve an uniform coagulation of the solder layer over the whole defect area. The minimization of the variations in the coagulation over the whole irradiated area was expected to lead to an increased tensile strength and decreased variation in the results.

2.2.2 Cartilage Samples

Calve knees from approximately four month old calves were obtained from a local abattoir (Metzgerei Meinen, Bern, Switzerland) . Shortly before the experiments, rectangular samples of an approximate size of 4 cm $\times$ 2 cm were prepared from the condylar articular cartilage. The samples consisted of cartilage connected to approximately 10 mm of the underlying bone. This was to ensure that the thermal properties during the experimental procedure mimic the clinical situation in situ as close as possible. After extraction from the joint the samples were placed in cooled (4 °C) phosphate-buffered saline (PBS: pH 7.4, NaCl 8.1 g, Na_2HPO_4 x 2 H_2O 0.984 g, NaH_2PO_4 x 2 H_2O 0.178 g, distilled water ad 1000 ml) to avoid desiccation.

The defects in the cartilage were prepared using a modified Zechner Drill with a diameter of 6 mm (see figure 2.3). The Zechner Drill consists of a sharp metallic tube sharpened at one end through which a flat drill was guided to millcut the defect. We fitted the tube with a metallic retainer which enabled us to cut a reproducible cavity of any chosen depth (1 mm or 1.5 mm in our experiments). Care was taken that the depth of the cartilage defect did not

reach the underlying bone (see figure 2.4).

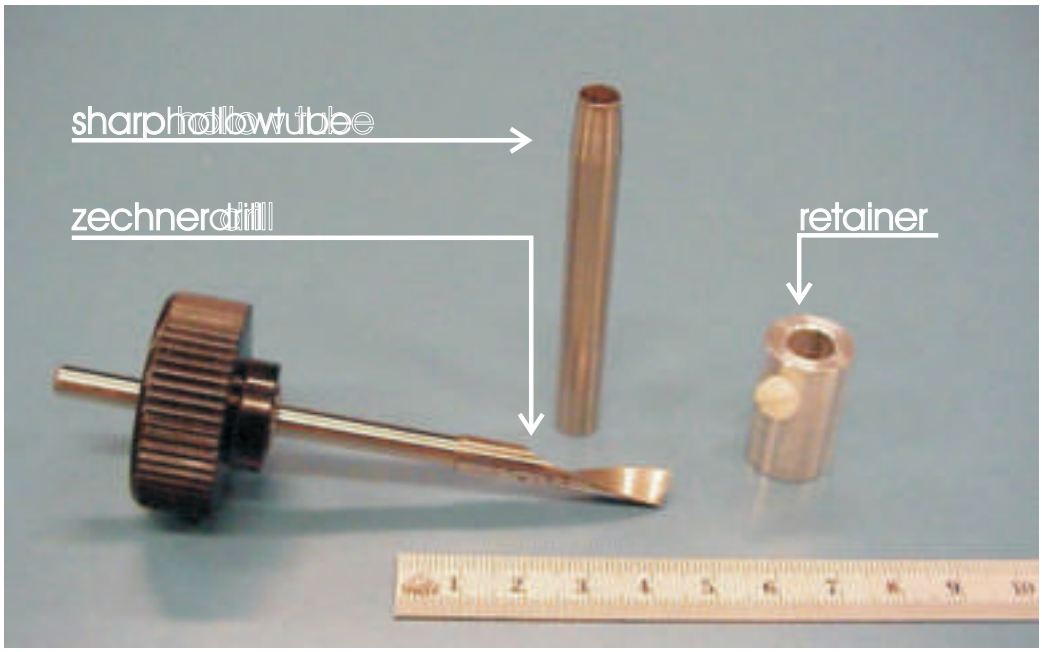

Figure 2.3: Zechner Drill with custom made retainer.

All the implants in this study were prepared using the sharp tube of the Zechner Drill to obtain cartilage discs that exactly match the geometry of the defect. The implanted cartilage discs were cut to a height of approximately 1 mm with the use of a scalpel (Model 10-155-18, martin, Tuttlingen, Germany) or microtome blade (Model 818, Leica Instruments GMBH, Nussloch, Germany). All cartilage implants have been cut in one preparation step before the soldering procedure started.

The bonding area for the implant in the defect is either only the bottom area or the bottom area plus the cylindrical walls of the cartilage defect. Thus we have a resulting bonding area A of $A{=}\pi r^2{=}0.282$ cm^2 if only the bottom is taken into account. If the walls of the cartilage defect are added the resulting bonding area is $A_{tot}{=}A + 2\pi rh{=}0.470$ cm^2.

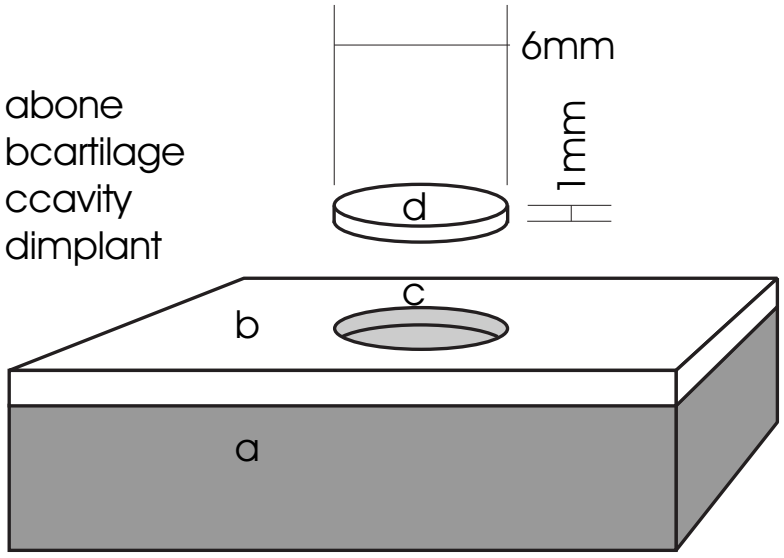

Figure 2.4: Cartilage sample with a piece of underlying bone.

2.2.3 Artificial Cartilage – Collagen Matrices

In addition to using fresh cartilage implants we used different collagen matrices provided and prepared by Centerpulse (Winterthur, Switzerland).

One of the main difficulties we encountered in prior experiments was, that the collagen matrices showed a poor temperature resistance and shrunk when irradiated by the laser.

The diameter of the matrices obtained was slightly smaller than the prepared cartilage defect. The thickness of the matrices was in some cases thicker than the depth of the defect (see figure 2.5) which led to an excess edge over the cartilage surface.

Collagen

Collagen is present in all multi-cellular organisms and exists in multiple variants. In mammals approximately 20 collagen genes can be found which all encode different forms of collagen. Collagens are the main constituents of

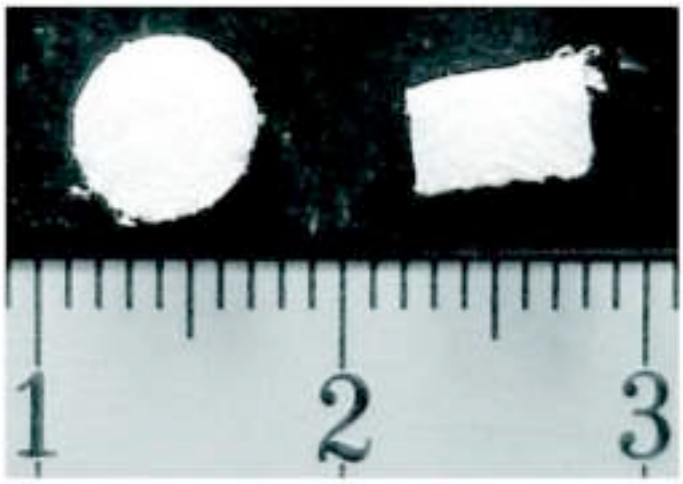

Figure 2.5: Top and side view of a collagen matrix.

bone, tendons and skin and account for 25 % of the whole protein mass of a mammal – more than any other protein.

A typical collagen molecule is a long, stiff, triple-threaded, helical structure. These collagen molecules assemble into ordered polymers called collagen fibrils, which are thin structures (10 to 300 nm in diameter and many micrometers long). The collagen fibrils often aggregate into larger cable-like bundles as collagen fibers of several micrometers in diameter. Other collagen molecules are attached to the surface of the fibrils and link the fibrils to each other and with other components of the extracellular matrix [13].

Collagen type I, II, III, V and XI are the main types of collagen found in connective tissues, the fibrillar collagen CI, CII, and CIII are among the most abundant proteins in the body.

Type I, the most common collagen type, is the principle collagen of skin and bone. Type I collagen is essential for the tensile strength of bone; the amount and distribution of these collagen fibers determines the size, shape and ultimate density of the bone. Type I is the major collagen of tendons and bones, but it is also the predominant collagen in lung, skin, dentin, heart

Type	Molecular Formula	Polymerized Form	Tissue Distribution
I	$[\alpha 1(I)]_2\alpha 2(I)$	fibril	Bone, skin, tendons, ligament, cornea, internal organ (account for 90 % of body collagen)
II	$[\alpha 1(II)]_3$	fibril	Cartilage, intervertebral disc, vitreous humor of the eye
III	$[\alpha 1(III)]_3$	fibril	Skin, blood vessels, internal organs

Table 2.1: Collagen types, Note that type I is composed of 2 types of α chains whereas types II and III are composed of only one type of a chain each.

valves, fascia, scar tissue, cornea, and liver.

Collagen type II is found predominantly, but not exclusively, in hyaline cartilage where it accounts for 90 % of the total collagen amount. Fibrils of type II collagen account for more than 50 % of dry weight of cartilage.

Type III collagen is found in small amount in many tissues in association with type I collagen, it is the major component of large blood vessels. It can also be found in several stromal[4] connective tissues including the dermis[5] of young organisms, human skin, and cornea. It can be used as a thin coating on tissue-culture surfaces to promote cell attachment and to modulate cell behavior.

2.2.4 Solder

We used a liquid Indocyanine Green (ICG) enhanced solder which was prepared with the use of sterile water, different concentrations of bovine serum albumin (BSA), ICG, hyaluronic acid (HA), and in some instances gelatin (Solder provided by Centerpulse, Winterthur, Switzerland). In total we used solders with 19 different variations of the ingredients. All concentrations

[4] *stroma* – The connective tissue framework of an organ, gland, or other structure.

[5] *dermis* – The sensitive connective tissue layer of the skin located below the epidermis - the outer, protective layer of the skin – containing nerve endings, sweat glands, blood and lymph vessels.

are given in weight per volume (i.e. 0.1 g ICG in 100 ml solder result in a concentration of 0.1 % ICG).

We studied a great number of different solders to evaluate the influence of the components (ICG, BSA, gelatin and HA) on the strength of the bond. ICG varied from 0.01 % to 1 %, BSA from 0 % to 50 %, HA from 0 % to 0.5 %, DEPC water[6] from 0 ml to 2.8 ml. The gelatin concentration varied from 0 % to 6.7 % in two different Bloom numbers[7] (180 g and 250 g). The absorption coefficient μ_a varied greatly from as low as 17 cm^{-1} for 0.01 % ICG to up to 763 cm^{-1} for 1 % ICG (the absorption curve has been obtained only once for each solder, therefore no error can be given).

The solders can be divided into three groups; first a group containing BSA as the bonding agent, then a second group containing gelatin as the bonding agent and a third group containing both BSA and gelatin.

ICG has a broad absorption peak ($\Delta\lambda$=60 nm, FWHM) with the maximum at 803 nm, thus absorbing at a wavelength which is poorly absorbed by water and bodily tissues. The absorption coefficient μ_a of our so called standard solder (0.1 % ICG, 25 % BSA and 0.5 % HA) was measured to be 231.6 cm^{-1} corresponding to an optical penetration depth δ of 43.2 μm. The solder was stored in a light-proof container in a refrigerator at approximately 4 °C and was allowed to reach room temperature before use.

Coagulation and denaturation of the albumin proteins contained in the BSA are the main bonding factors. ICG binds preferentially with serum protein ensuring that heat is efficiently transferred to denature the protein

[6]DEPC-treated water is deionized, high quality, molecular biology grade water, for use in all molecular biology experiments.

[7]The Bloom value of a gelatin is defined as the force required for a plunger of defined shape and size to make a depression in a gel that has been prepared at a 6.67 weight-% solution and has been kept in a constant temperature bath at 10 °C for 18 hours. If the required force for this procedure is 250 grams, then the gelatin is a 250 g Bloom gelatin.

solder generating the desired fusion between the solder and the cartilage.

Hyaluronic acid is ubiquitous in the organism where it plays an important biological role. The highest concentrations are found in soft connective tissue where it is a major component of the extracellular matrix, and in the vitreous body of the eye. HA is present in hyaline cartilage, in synovial joint fluid and in the skin tissue, both dermis and epidermis. Until recently, HA was considered to be an inert space filler that fulfilled only mechanical roles in the human body. This situation has radically changed since HA has been demonstrated to modulate acute and chronic inflammation processes both in animals and human beings [14]. HA was added to the solder to provide a known environment to the soldered tissue.

Gelatin's ability to form thermo-reversible gels, its amphoteric[8] character, and contribution to viscosity make it an ideal thickener, adhesive agent and stabilizer or emulsifier. The gelatin was added to the solder to vary the viscosity. The decrease in viscosity helped with the application of the solder. In the first experiments we encountered problems to disperse the solder uniformly in the cartilage defect, through surface tension the solder was quickly accumulated in the edges of the cavity in the cartilage. We wanted to have different viscosities of the solder to see if there is an influence on application, thus if the solder does not as easily flow into the edges of the damage as before.

[8] *amphoteric* – Having the characteristics of an acid and a base and capable of reacting chemically either as an acid or a base.

2.2.5 Soldering Procedure

Preliminary Experiments and First Part of the Experiments

Due to an optical penetration depth δ of 2.9 mm at a wavelength λ of 810 nm [15] irradiation of the solder is possible through the thin implant and – with a thin layer of low absorption solder – through the solder onto the underlying cartilage. Furthermore the thermal injury in the cartilage adjacent to the strongly absorbing solder layer (μ_a=231.6 cm^{-1} for the standard solder) is solely a result of heat conduction from the solder to the cartilage. This thermal damage scales with the irradiation time and deposited energy and is confined to surfaces covered by the solder.

We applied the solder with the use of a 1 ml single use syringe and an injection needle in three steps:

- First a solder layer – called the base coating – was applied as thin as possible into the prepared cartilage defect (see figure 2.4), which was then irradiated with the 808 nm diode laser. The amount of solder was recorded as either small, normal or big. The time necessary to coagulate the solder was evaluated in a preliminary experiment. Through visual control the end point was evaluated. The solder layer changes color and the scattering of light in the solder increases greatly at the point where coagulation occurs. When hand-guiding the bare fiber over the solder-covered cartilage defect, the coagulation of the whole solder layer is strongly dependent on the fiber movement.

- After the first irradiation a second solder layer was applied on top of the first one. The prepared implant was fitted into the cartilage defect and the solder was then irradiated through the cartilage implant on top (this step was called implant irradiation).

- Finally a third layer of solder was applied at the circular boundary of the implant (green ring seen in figure 2.7) and irradiated (this step was called boundary irradiation).

Since pilot experiments revealed a large variation in tensile strength of the implant, care was taken to keep a high reproducibility.

Second Part of the Experiments

In the second set of experiments the solder was applied with the use of a 1 μl and a 5 μl micropipette (Oxford Laboratories Sampler, Kontron Technik AG, Switzerland) to facilitate the application of a reproducible amount of solder.

To ensure a reproducible thickness of our implants – which seemed to contribute to the large variation observed in the first part of the soldering experiments – we used a special cutting jig (see figure 2.6). This showed to have a positive influence on the variation in our results.

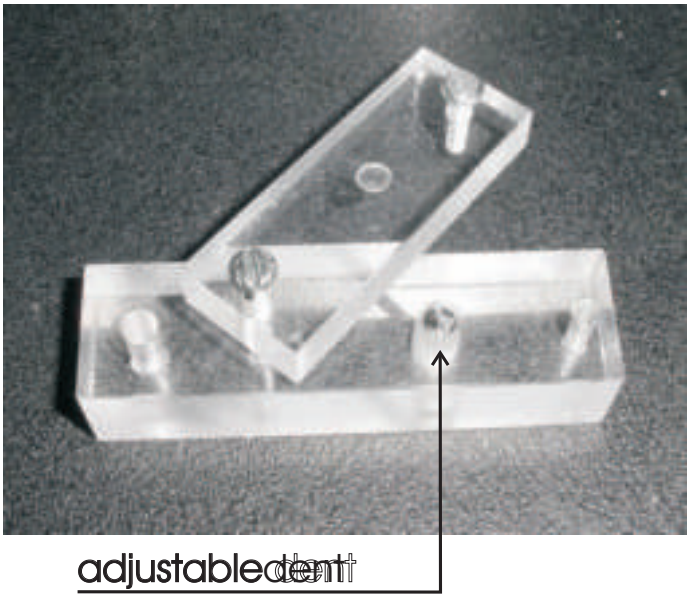

Figure 2.6: Jig used to cut the implants.

The implants were prepared in the same manner as in the first part of the experiments, but then cut to identical thickness using the aforementioned jig. The matrices were inserted in the adjustable dent of the jig and then cut to the desired height by sliding a microtome blade (Model 818, Leica Instruments GMBH, Nussloch, Germany) through the slit in the jig, which resulted in an exactly coplanar implant of a defined height.

2.2.6 Tensile Strength Evaluation

Subsequent to the soldering experiments the tensile strength was measured using a calibrated force gauge (AFG-100N from Mecmesin, Slinfold, United Kingdom). The sample was clamped to the laboratory table and a pulling rod with a diameter of 4 mm was glued onto the soldered cartilage implant using Cyanoacrylate (Zap-a-Gap, Pacer Technology, California, USA). The rod was connected to the force gauge mounted on a motorized bench vice (Centerpulse, Winterthur, Switzerland). The implant was pulled apart at a constant speed of 25 mm/min until breakage occurred and the maximal force recorded (see figure 2.7).

2.2.7 Tissue Viability – Live/Dead-Staining

As published earlier, all standard staining and histology methods (Safranin-O, Alcasian-Blue and Masson-Trichrome, van Gieson and Haematoxylin/Eosin Staining) reveal only about half of the damage zone found with the Live/Dead viability test [4, 16, 17].

The Live/Dead assay is a two-color fluorescence-based cell viability test that allows the simultaneous determination of live and dead cells. Live cells are identified by the presence of ubiquitous intracellular esterase[9] activity,

[9] *esterase* – Any of various enzymes that catalyze the hydrolysis of an ester.

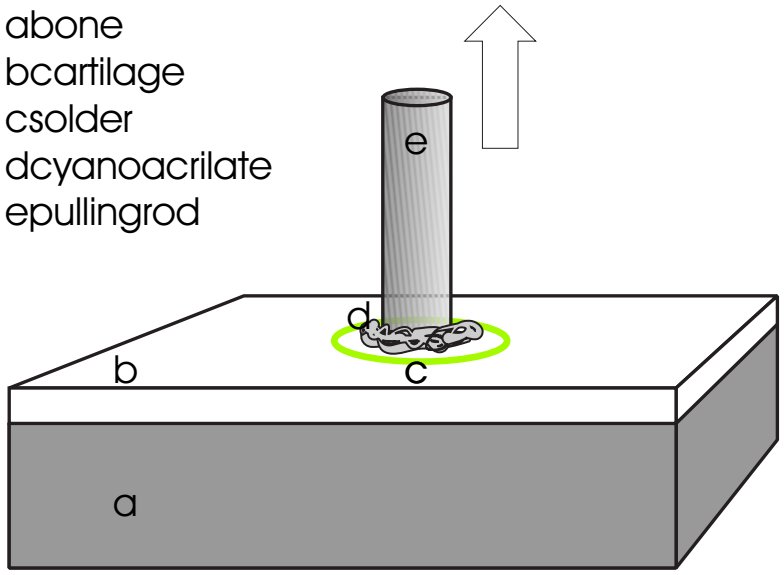

Figure 2.7: Preparation for tensile strength measurement.

and dead cells are identified by the lack of plasma membrane integrity.

Calcein acetoxymethyl (calcein AM) is a virtually non-fluorescent cell-permeant esterase substrate which has the ability to distribute into the cytoplasm[10] of viable cells where it is hydrolyzed to the highly fluorescent calcein, which is retained within live cells and produces an intense uniform green fluorescence in live cells (excitation wavelength ∼495 nm, emission wavelength ∼515 nm). Therefore, green fluorescence is an indicator for viable cells since calcein AM can only be loaded into living chondrocytes where the plasma membranes are intact and intracellular processes maintained.

Ethidium homodimer-1 is a nucleic acid stain which enters cells with damaged membranes and binds to both DNA and RNA, producing a bright red fluorescence (excitation ∼495 nm, emission ∼635 nm). This dye is excluded from cells that have intact plasma membranes but is able to enter dead cells. It can therefore be used to label the nuclei of damaged and dead

[10] *cytoplasm* – The entire contents of a live cell exclusive of that of the nucleus.

cells in which plasma membrane integrity and cellular metabolism have been compromised. Thus, live cells fluoresce green, while dead cells fluoresce red.

Background fluorescence levels are inherently low with this assay technique because the dyes are virtually non-fluorescent before interacting with cells.

Following the laser soldering procedure the samples were kept in PBS to minimize environmental influences. After soldering, the cartilage layer with the implant was removed from the underlying bone and cut to a smaller size (approximately 1 cm $\times$ 1 cm $\times$ 3 mm). The removed cartilage was afterwards embedded in 3 % Agar (Fluka Chemical, Buchs, Switzerland) suspended in PBS and then sectioned into either 150 μm or 200 μm thick slices by means of a fresh-tissue sectioner (Sorvall TC-2, Smith & Farquhar, Newtown, USA). The slices were then incubated in calcein AM and ethidium homodimer-1 (Live/Dead Viability/cytotoxicity Kit, Molecular Probes, Eugene, Oregon, USA) for 1 hour.

After incubation the cartilage slices were analyzed with a confocal laser scanning microscope (CLSM, Zeiss LSM 410 invert, Zeiss, Oberkochen, Germany). To confirm the proper functioning of the viability assay no separate controls were necessary since the viable cells emitting green fluorescent light next to the damaged red fluorescing area in each micrograph were considered as control.

An important prerequisite for testing the chondrocyte viability in cartilage is the use of fresh cartilage and proper handling throughout the experimentation procedure. All steps for the Live/Dead test, the dissection, the soldering experiments, incubation and analysis with the Laser Scanning Microscope were made within nine hours. Between the single manipulation steps the samples were stored in PBS to avoid desiccation.

2.3 Monte-Carlo-Simulation

To be able to quantify the absorbed, scattered and reflected light we used a Monte-Carlo-simulation. To simulate the light distribution, the software chooses random numbers which are used along with the parameters of interest (absorption and scattering coefficients μ_a and μ_s, anisotropy factor g, etc.) to determine the positions at which scattering events occur. With the calculated angle of scattering, the software is able to simulate the light distribution in the cartilage tissue.

For the simulation, the tissue was assumed to consist of three layers, irradiated with a collimated beam with a diameter of 6 mm. Because of the sample being symmetrical to the beam axis, only a section is shown in figure 2.8.

The tissue parameters can be found in an article from Ebert et al. [15]. For all wavelengths between 300 nm and 850 nm articular cartilage possesses very weak absorption properties with scattering dominating absorption. At the wavelength of 810 nm the values of the absorption coefficient μ_a and scattering coefficient $\mu_s^{'}$ are μ_a=0.75 cm^{-1} and $\mu_s^{'}$=11 cm^{-1}.

The reduced scattering coefficient $\mu_s^{'}$ can be calculated from the scattering coefficient μ_s using the formula below.

$$\mu_s^{'} = \mu_s(1-g) \tag{2.4}$$

The scattering coefficient μ_s calculated from $\mu_s^{'}$=11 cm^{-1} is thus μ_s=120.9 cm^{-1}.

For rabbit cartilage tissue the anisotropy factor g is 0.909 $\pm$ 0.005 [18] which was the value we used in our calculations.

Table 2.2 summarizes the parameters used for the Monte-Carlo-

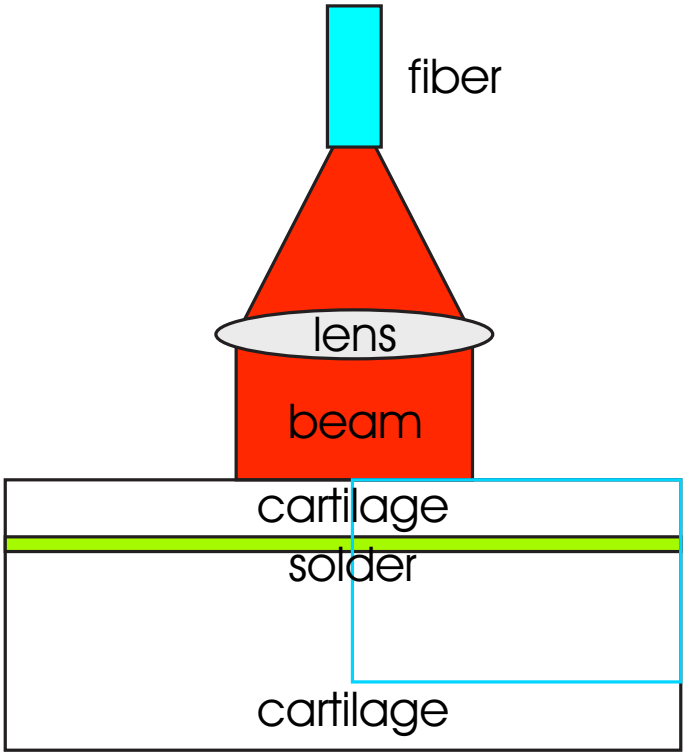

Figure 2.8: Monte-Carlo-simulation. The blue rectangle seen in the cartilage sample matches with the figure area seen in the Monte-Carlo-simulation (figures 2.9 to 2.11).

simulation. Figure 2.9 shows the resulting absorption and fluence distribution for two solders having a low (16.9 cm^{-1}) and a high (763.1 cm^{-1}) absorption coefficient μ_a.

	layer	μ_a [cm‘$^{-1}$]	μ_s [cm^{-1}]	g	n	layer thickness [cm]
1	cartilage	0.75	120.9	0.909	1.4	0.1
2	solder	desired μ_a	0.1	0.9	1.3	0.02
3	cartilage	0.75	120.9	0.909	1.4	0.5

Table 2.2: Monte-Carlo-simulation parameters

The situation is the same in all the pictures; a cartilage layer of 0.1 cm is followed by a solder layer of 0.02 cm which is then backed by the underlying solder layer.

The difference between the solder with a low μ_a (figures 2.9(a) and 2.9(b))

and the one with a very high μ_a (figures 2.9(c) and 2.9(d)) is clearly visible. In the top left figure the energy is absorbed through the whole solder layer, while in the top right figure the energy is only absorbed in the uppermost part of the solder.

Figure 2.9(b) shows that using a low absorbing solder, a considerable part of the energy is not absorbed in the solder and transferred to the underlying cartilage layer.

As expected the different solders showed a strong absorption dependence on the different ingredients. The biggest difference expectedly arose from the ICG-concentration which directly affects the absorption of the solder.

A noticeable difference occurs when the incident beam is not gaussian, but rather a tophat profile, the irradiation over the whole sample area is much more homogeneous as opposed to irradiation with a gaussian beam (compare figures 2.9 and 2.10).

The so-called standard solder (0.1 % ICG, 25 % BSA and 0.5 % HA) with a μ_a of 211.5 cm^{-1} showed an intermittent behavior as can be seen in figure 2.11. Only a fraction of the energy passes through the uppermost solder layer (the whole layer is 200 μm thick)

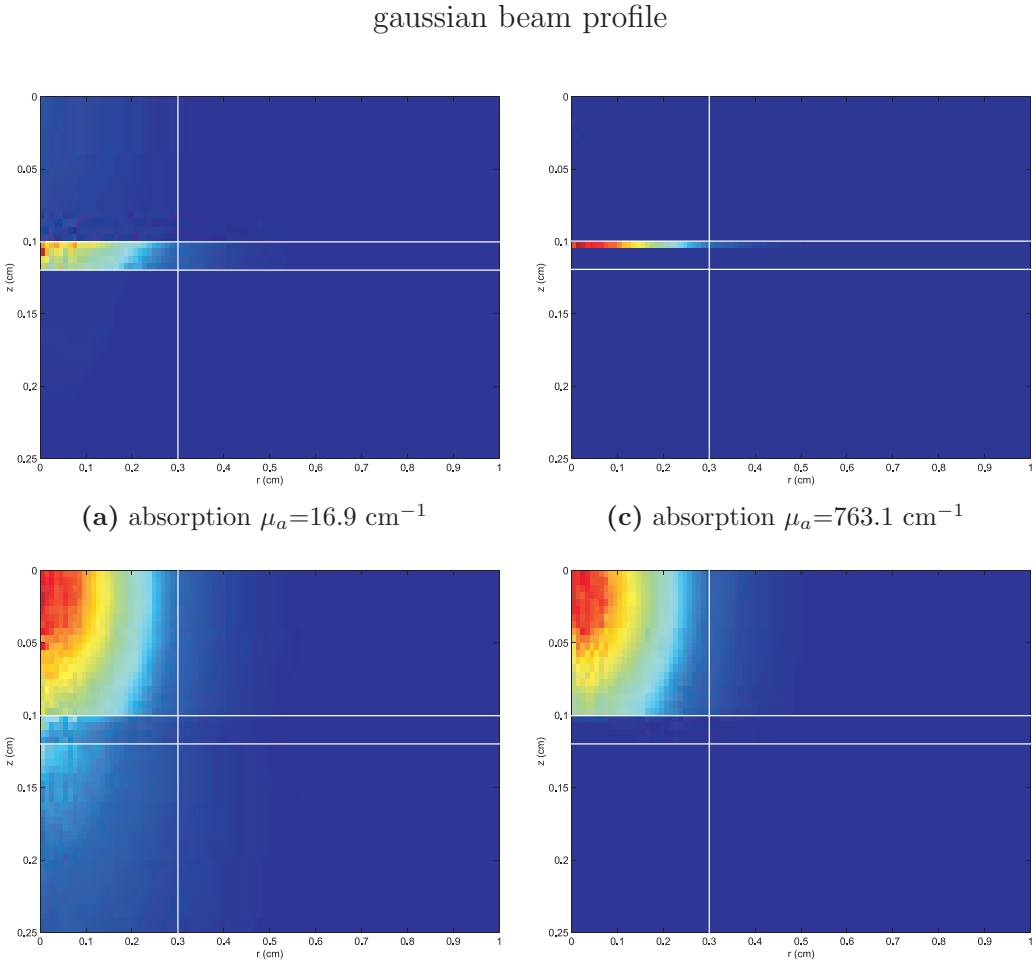

(a) absorption μ_a=16.9 cm^{-1}

(c) absorption μ_a=763.1 cm^{-1}

(b) fluence μ_a=16.9 cm^{-1}

(d) fluence μ_a=763.1 cm^{-1}

Figure 2.9: Absorption and fluence simulations with a gaussian beam profile. Pictures (a) and (b) show a solder with a μ_a of 16.9 cm^{-1}, pictures (c) and (d) show a solder with a μ_a of 763.1 cm^{-1}. Both top figures show the absorption, the bottom figures the fluence. In these and all the following Monte-Carlo-simulation figures the two horizontal white lines mark the border between solder and cartilage and the vertical line marks the beam radius.

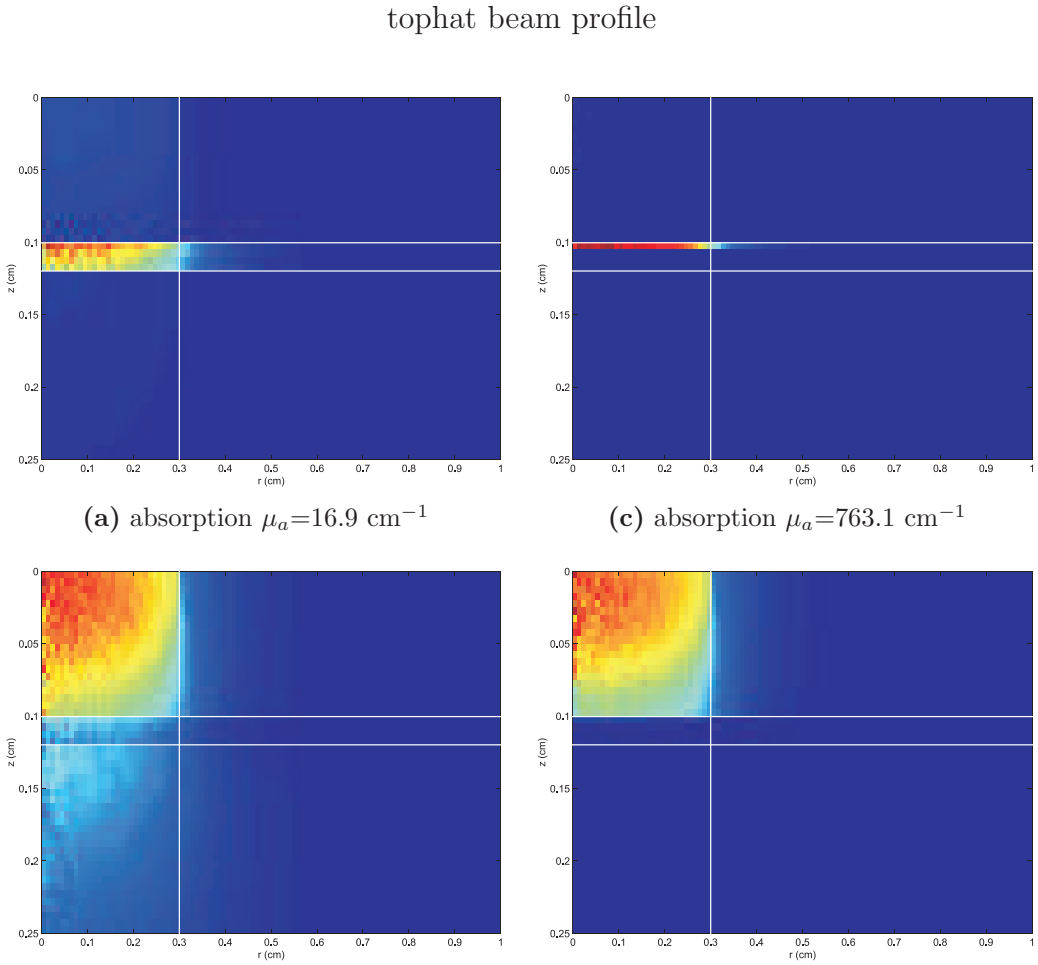

(a) absorption μ_a=16.9 cm^{-1}

(c) absorption μ_a=763.1 cm^{-1}

(b) fluence μ_a=16.9 cm^{-1}

(d) fluence μ_a=763.1 cm^{-1}

Figure 2.10: Absorption and fluence simulations with a tophat beam profile. Pictures (a) and (b) show a solder with a μ_a of 16.9 cm^{-1}, pictures (c) and (d) show a solder with a μ_a of 763.1 cm^{-1}. Both top figures show the absorption, the bottom figures the fluence.

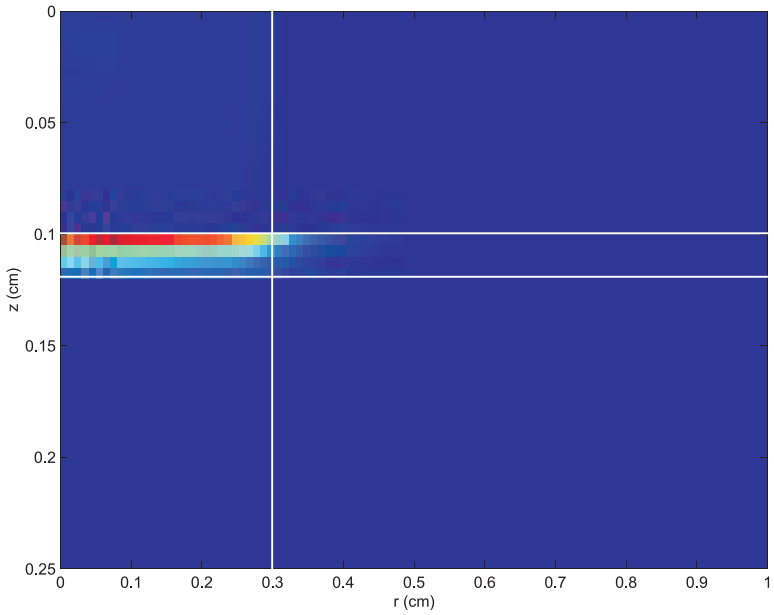

(a) absorption μ_a=211.5 cm^{-1}

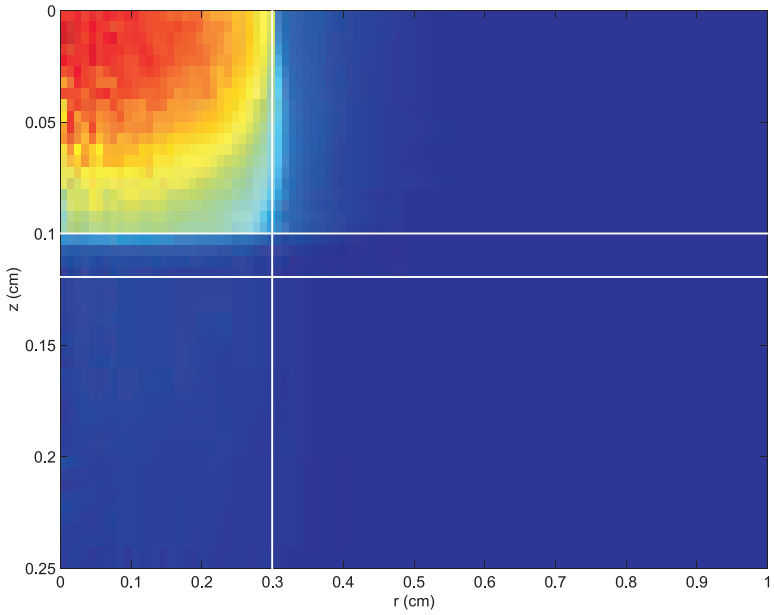

(b) fluence μ_a=211.5 cm^{-1}

Figure 2.11: Absorption and fluence of a solder with a μ_a of 211.5 cm^{-1}, irradiated with a tophat beam profile.

2.4 Results

2.4.1 Influence of Solder Ingredients on Tensile Strength

The ICG-concentration, the main factor influencing the absorption in the solder, was varied from 0.01 % to 1 % ICG corresponding to a measured absorption coefficient μ_a of the solder ranging from 16.9 ± 4 cm^{-1} to 759 ± 10 cm^{-1}.

The following ICG-concentrations were used: 0.01 %, 0.04 %, 0.08 %, 0.1 %, 0.2 % and 1 %.

The optimal concentration of ICG in view of tensile strength was found to be 0.1 %, as shown in figure 2.12. This value produced the highest tensile strengths 1.15 ± 0.78 N for 50 % BSA and 0.70 ± 0.53 N for 25 % BSA and the highest absolute values 3.23 N and 2.07 N for 50 % and 25 % BSA, respectively. All other concentrations showed far lower values.

Table 2.3 and figure 2.12 summarize the obtained results.

ICG [%]	BSA [%]	mean tensile strength [N]	standard deviation	number of samples
0.01	25	0.37	0.27	3
0.04	25	0.37	0.13	3
0.1	25	0.70	0.53	24
1	25	0.43	0.18	5
0.1	50	1.15	0.78	62

Table 2.3: Tensile strength depending on ICG- and BSA-concentration.

Besides varying the ICG-concentration we also tested solders at a fixed ICG-concentration but with either 25 % or 50 % bovine serum albumin. The optimal concentration of BSA for the soldering of cartilage was found to be 50 %. For this concentration we were able to achieve the highest tensile strength (1.15 ± 0.78 N) and the highest absolute value of 3.23 N.

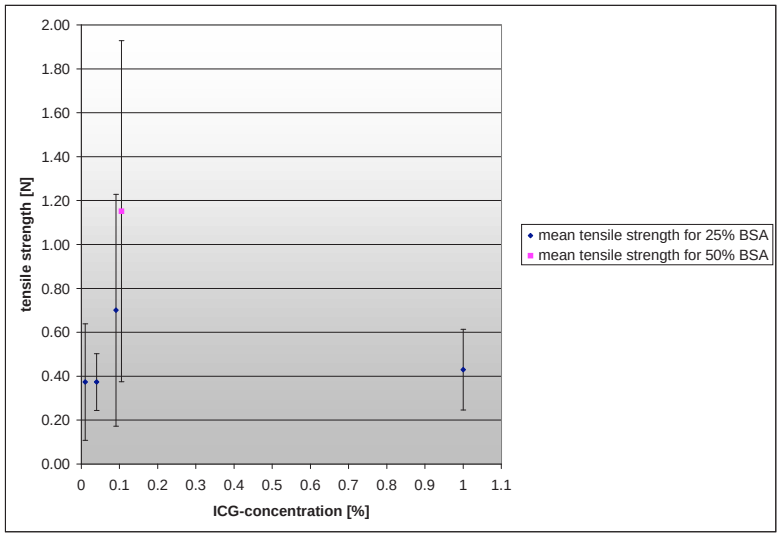

Figure 2.12: Tensile strength with standard deviation as a function of ICG-concentration of the solder after cartilage soldering.

Table 2.4 and figure 2.13 summarize the obtained results for an ICG-concentration of 0.1 %.

BSA [%]	mean tensile strength [N]	standard deviation	number of samples
25	0.70	0.53	24
50	1.15	0.78	62

Table 2.4: Tensile strength depending on BSA-concentration, for an ICG-concentration of 0.1 %.

Solders containing 0.5 % gelatin in addition to BSA resulted in a tensile strength of 0.60 ± 0.45 N for 25 % BSA (11 samples in total) and 1.26 ± 0.97 N for 50 % BSA (12 samples).

Varying the concentration of hyaluronic acid in the solder had no influence on the tensile strength of the soldered bond.

The tensile strength measurements performed with solders containing exclusively gelatin as bonding agent, resulted in a maximum tensile strength value of only 0.12 N (for the solder with the highest gelatin concentration,

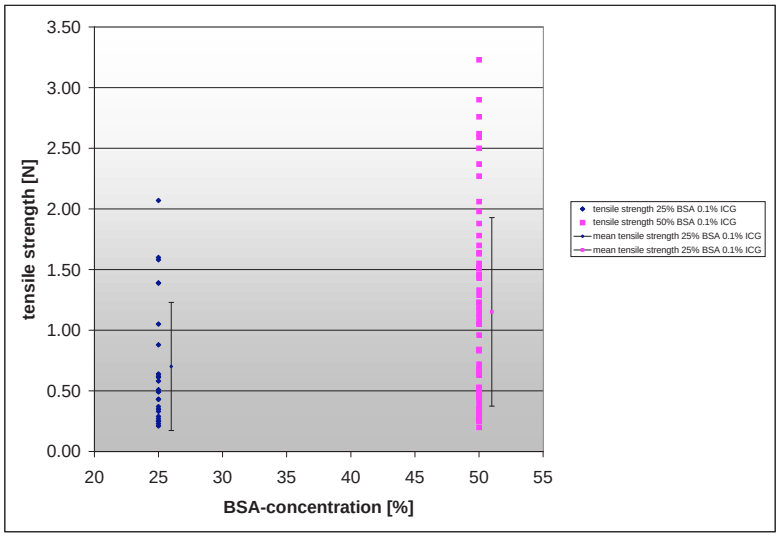

Figure 2.13: Tensile strength and mean tensile strength with standard deviation as a function of BSA-concentration for a fixed ICG-concentration of 0.1 % after cartilage soldering.

6.7 %) therefore we discontinued the measurements with these solders.

In total we conducted 142 pulling experiments with 13 different solders. Tensile strength measurements leading to a result lower than 0.2 N were considered as total failure and not counted, therefore we had 97 measurements.

The results admits of two conclusions (see also [19]):

- Choosing an ICG-concentration of 0.1 % leads to repairs with highest tensile strength.
- Increasing BSA-concentration from 25 % to 50 % improves the tensile strength of the repair by 65 % (0.70 N and 1.15 N, for 25 % and 50 % BSA, respectively).

2.4.2 Matrices

The soldering experiments using a collagen matrix as implant showed less promising results. In total we conducted 25 pulling experiments with collagen

matrices implanted in cartilage. Only one of them led to a tensile strength result bigger than 0.2 N (0.23 N).

One of the main difficulties was the shrinkage of the collagen matrices which occurred while irradiating the solder underneath. This shrinkage prevented a strong bond between underlying cartilage and collagen matrix (see figure 2.14).

Figure 2.14: Irradiated cartilage defect with extremely shrunken matrix (irradiated with 1.5 W for 30 s and with 1.5 W for 90 s, base coat and implant irradiation, no boundary irradiation has been performed with this sample).

Another difficulty arose from the porosity of the matrices, causing the liquid solder to get soaked into the collagen matrix. Therefore, most of the irradiated laser light is already absorbed inside the matrix and not exclusively in the solder-filled gap between the matrix and the cartilage. This leads to a strong heating of the matrix and finally to its shrinkage as shown in figure 2.14. This strong temperature rise also caused desiccation and subsequent carbonization of the solder, preventing a good bond of the collagen matrices with the underlying defect (the carbonization can also be seen on the left side of the matrix in figure 2.14).

To overcome the diffusion problem, a few experiments have been made with a collagen membrane (BioMend, Colla-Tec Inc., Plainsboro, USA) doped with solder prior to the insertion into the cartilage defect. Although the thin membrane prevented diffusion of solder into the matrix, it could not be soldered to the collagen matrix, nor to the underlying cartilage.

2.4.3 Thermally Induced Tissue Damage

In addition to the samples used for tensile strength measurements, we prepared another set of samples to determine the laser-induced thermal damage in the cartilage.

The thermal damage of the cartilage tissue is induced only through heat diffusion from the solder to the cartilage tissue.

The mechanical tissue damage generated through the preparation of the samples is not visible in the Live/Dead pictures. This damage induced through the Zechner Drill and the Zechner Drill tube which were used to prepare the implants is lower than the thermal damage induced through the absorption of the laser irradiation in the solder. To be able to quantify the mechanical damage for the samples, a sample has been assessed with the Live/Dead-test which was not irradiated with the laser. The damage induced through the preparation was found to be around 100 μm for the border of the implant and around 180 μm for the bottom and border of the cartilage defect, (for explanation of the terms see figure 2.15), while the thermal damage was at least 215 μm for the border or 610 μm for the bottom of the cartilage defect.

The thermal damage found at the bottom of the defect was – depending on the deposited laser power and irradiation time – between 610 μm in the case of low energy irradiation and short time (0.85 W, 30 s, base coat, 1.58 W,

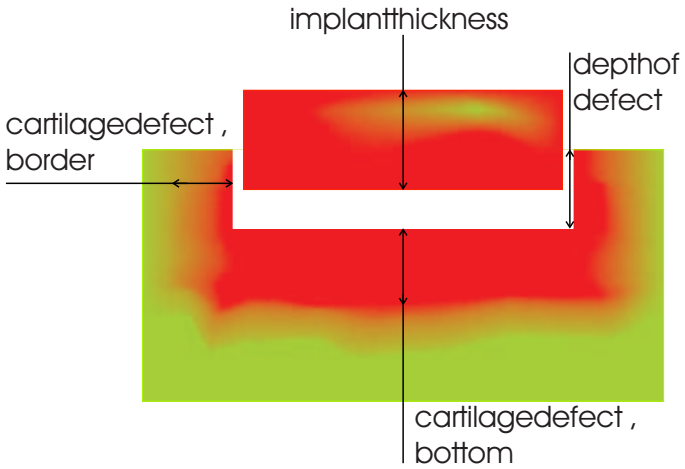

Figure 2.15: Live/Dead-Terminology

Solder composition [%]			I_{BC}	t_{BC}	I_I	t_I	I_B	t_B	S_{ten}	D_{max}
ICG	BSA	gelatin	[W]	[s]	[W]	[s]	[W]	[s]	[N]	[μm]
0.1	25	0	30	0.85	65	1.58	45	0.85	1.39	610
0.1	25	0	60	1.30	90	1.96	60	1.30	1.05	785
0.1	50	0	60	1.30	90	1.96	60	1.30	1.25	1196
0.1	25	0.5	60	1.30	90	1.96	60	1.30	1.05	1268
0.1	50	0.5	60	1.30	90	1.96	60	1.30	1.16	1477
0.1	50	0.5	30	1.58	60	1.96	45	1.58	1.05	1028
0.1	25	0.5	45	1.58	60	1.96	45	1.81	1.39	1338
0.1	50	0	45	1.81	65	2.38	45	1.81	0.34	1831

Table 2.5: Details of thermal damage evaluation, I_{BC} is the base coat irradiation power, I_I and I_B are the irradiation power for the implant irradiation and boundary irradiation, t_{BC}, t_I and t_B are the irradiation times for the three irradiation steps. Tensile strength S_{ten} and D_{max}, which denotes the maximal thermally induced damage at the cartilage defect bottom have been evaluated in two different sets of experiments with the exact same settings.

45 s, implant and 0.85 W, 45 s, boundary irradiation) and 1831 μm in the worst case, thus with a high laser power (1.81 W, 45 s, base coat, 2.38 W, 65 s, implant and 1.81 W, 45 s, boundary irradiation), see also table 2.5.

Figure 2.16 and figure 2.17 show pictures of these two extreme cases obtained with the confocal Laser Scanning Microscope. Since the samples were too large to be captured in one image, we took several pictures of the

same sample and combined them using an image program (Corel PHOTO-PAINT).

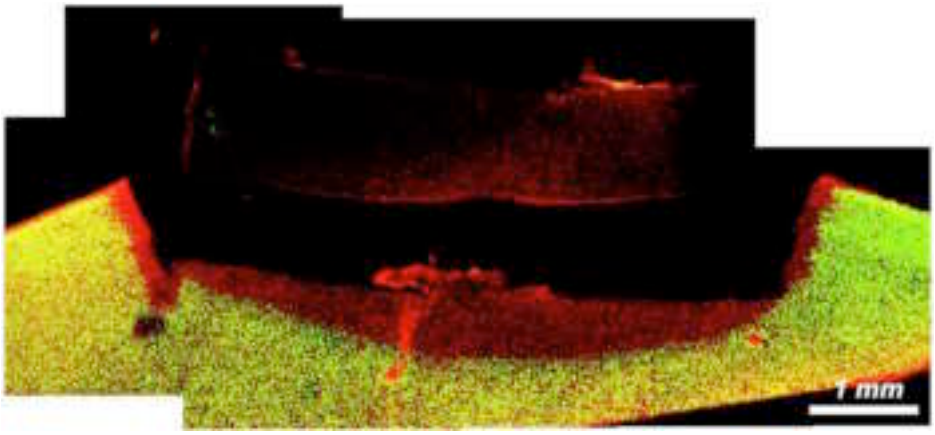

Figure 2.16: Live/Dead picture, Solder 0.1 % ICG, 25 % BSA, 0.5 % HA, irradiated 30 s with 0.85 W, 45 s with 1.58 W and 45 s with 0.85 W, (base coat, implant irradiation and boundary irradiation). The picture was electronically put together from different single pictures. The separation of the implant is an artefact caused by sample preparation.

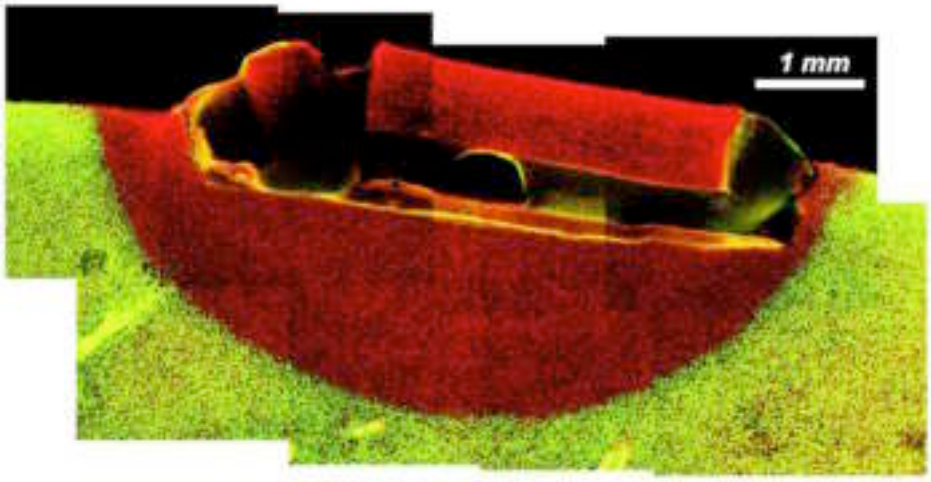

Figure 2.17: Live/Dead picture, Solder 0.1 % ICG, 50 % BSA, 0.5 % HA, irradiated 45 s with 1.81 W, 65 s with 2.38 W and 45 s with 1.81 W, (base coat, implant irradiation and boundary irradiation), left part of the implant is damaged through wrong cutting procedure. The picture was electronically put together from different single pictures.

2.5 Discussion

2.5.1 Monte-Carlo-Simulation and Tensile Strength

The goal of the present study was to determine laser and solder parameters able to solder cartilage to cartilage with a high – and at the same time – reproducible tensile strength. In order to optimize the soldering process, the influence of ICG-concentration on the spatial distribution of absorbed laser light was determined using Monte-Carlo-simulations. These simulations revealed that due to the low absorption of 808 nm radiation in cartilage (μ_a=3.45 cm^{-1} [15]) the radiation is almost exclusively absorbed in the ICG of the solder layer. The simulation further showed that the absorption in the solder varies greatly with the ICG-concentration. This variation leads to an inhomogeneous coagulation of the solder and an inhomogeneous deposition of heat in the tissue. An almost homogeneous absorption in the entire solder layer was found for an absorption coefficient μ_a of approximately 200 cm^{-1} corresponding to an ICG-concentration of 0.1 %.

If the ICG-concentration is chosen too high, the absorption in the solder is extremely high, leading to an absorption of the irradiated laser energy in the very top layer of the solder (see figure 2.9). This strong temperature gradient in the solder layer promotes an inhomogeneous coagulation of the solder, finally leading to a low tensile strength.

If the ICG-concentration is very low, then a longer irradiation time is needed to rise the temperature in the solder layer above the coagulation value of approximately 70 °C. Due to heat diffusion, the adjacent cartilage desiccates and shrinks, which makes a strong connection between implant and cartilage layer impossible.

The Monte-Carlo-simulation further revealed, that irradiating the sample

with a tophat profile leads to a more uniform absorption of the radiation in the solder layer and therefore to a more homogeneous coagulation of the solder than after irradiation with a Gaussian beam profile.

These theoretical considerations were perfectly confirmed by the experimental results as shown in figure 2.12.

The 0.1 % ICG-concentration represents a kind of compromise between homogeneous energy deposition across the solder layer and a fast temperature rise above 70 °C necessary for a good and strongly soldered connection. This compromise can be made responsible for the fact that the implant-solder connection was found to be stronger than the solder-cartilage connection, between which the soldered sample got ripped off in 80 % of the tensile strength measurements.

A main problem arising during the soldering procedure was an uneven distribution of the solder layer in the cartilage defect. Most of the liquid solder was caused to accumulate at the edge of the defect by surface tension. To circumvent this problem we increased the viscosity of the solder either by increasing the BSA-concentration or by adding gelatin to the solder.

The results show that a concentration of 50 % BSA in the solder seems to be ideal to achieve high tensile strengths. A high concentration of BSA has two positive effects: First, a higher concentration of albumin in the solder leads to an increasing viscosity, which means that the solder can be applied homogeneously in the cartilage defect. And secondly a solder containing a high albumin-concentration allows more proteins to denaturate through irradiation, leading to more connections in the solder and between solder and cartilage, and to a high tensile strength.

Adding gelatin instead of BSA to the solder to increase the viscosity caused different problems. During and following irradiation the solder be-

came brittle and dried out extremely fast, which in some cases led to carbonization of the solder in the cartilage defect.

Although the gelatin solder had an almost optimum consistency to obtain a homogeneous solder layer in the defect the tensile strength measured was extremely low (maximum tensile strength lower than 0.2 N) and therefore discarded as a not usable soldering result.

The solders containing very little gelatin (0.5 %) in addition to BSA showed none of these drawbacks. A negative effect of the gelatin was not perceivable. We used some of these solders in the Live/Dead-assay to evaluate a difference in tissue damage but could not find a significant difference between solders containing little gelatin and solders containing no gelatin.

Considering the three groups of solders (containing either BSA, BSA and gelatin or only gelatin as a main bonding factor), all having an ICG-concentration of 0.1 % we can conclude:

- BSA is responsible for the soldering process, creating a tensile strength that increases with increasing BSA-concentration.
- Solders containing a low gelatin concentration with BSA showed no perceivable difference in tensile strength measurements to solders containing the same BSA-concentration without gelatin.
- Solders containing only gelatin without BSA can not be used due to the low tensile strength obtained.

2.5.2 Thermally Induced Tissue Damage

The examination of soldered cartilage junctions by confocal laser scanning microscopy showed good albumin-tissue connection, mostly on the boundary between solder and cartilage implant. The thermal and mechanical tissue

damage can unequivocally be determined with a Live/Dead staining technique. Layers of dead chondrocytes can easily be distinguished from viable cells by their different fluorescence (see figure 2.18).

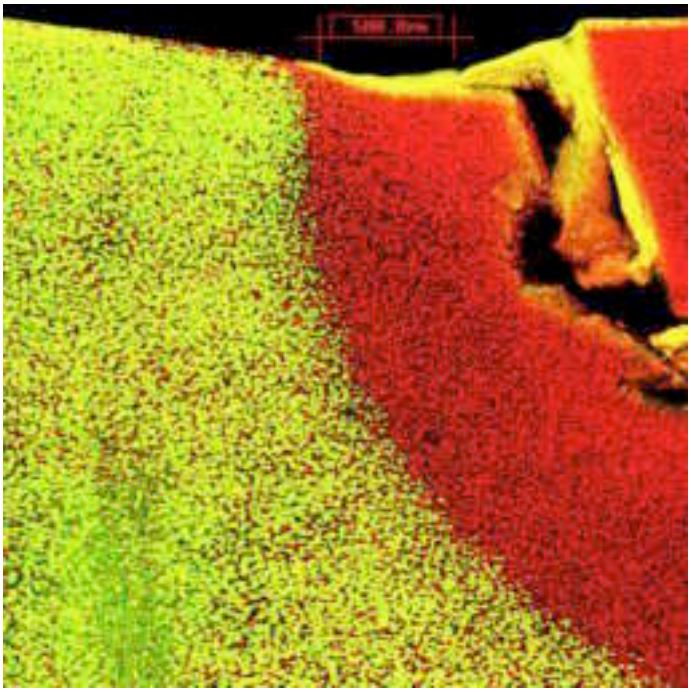

Figure 2.18: Live/Dead picture, viable cells are green, dead cells are read, the solder is yellow.

Heat diffusion led to thermally damaged zones on both sides of the heated solder layer. The cell damage threshold has been shown to be 54 °C (heating cartilage in a heat bath for 5 minutes [3]). Since the laser soldering process lasted much shorter (30 to 90 s), we can assume that a minimal temperature of 54 °C was reached at the transition from the red to the green zone.

The implant was practically fully damaged in all the Live/Dead-Test we evaluated. The implant damage is in all cases bigger than the thermal damage of the defect bottom. The damage is partially from an inhomogeneous absorption in the solder, which happens only in the top layer of the solder, while the cartilage defect below is partially shielded by the not fully

coagulated solder.

If we consider the power in each irradiation step (base coat, implant irradiation and boundary irradiation) the tissue damage directly scales with the laser power and irradiation time. The so called base coat irradiation (the irradiation of the solder layer in the defect without the implant on top) and the implant irradiation (implant fitted into the defect) seem to have the biggest influence on the thermally induced tissue damage.

The thermal damage has only been assessed with solders containing 0.1 % ICG, which led to high tensile strength results.

The thermal damage was found to scale with the concentration of BSA in the solder. For experiments with identical irradiation parameters but different BSA-concentration (25 % and 50 %) we found a difference in the thermally induced tissue damage of 411 μm (785 μm and 1196 μm) and in the case of two other samples we found a difference in thermally induced tissue damage of 209 μm (1268 μm and 1477 μm).

Solders containing a high amount of BSA seem to facilitate the heat diffusion from the solder into the cartilage leading to a higher thermal damage on the one hand and on the other hand lead to higher tensile strength measurements.

The thermal damage found is overall bigger than the thermal damage that has been assessed before [3], leading to the conclusion that though the irradiation over the whole area of the cartilage defect leads to a higher reproducibility of the tensile strength measurements, the prolonged irradiation time on the other side leads to an increased thermally induced tissue damage.

2.6 Conclusions

Cartilage tissue can be soldered with the use of a 808 nm diode laser and an Indocyanine Green enhanced albumin solder. The solder allows the optimization of absorption properties by changing the dye concentration. Through the choice of high BSA-concentration of 50 % the strength of the bond between the implant – either cartilage or artificial tissue – and the underlying joint cartilage can be increased compared to concentration of 25 % serum albumin.

The thermal damage induced in the cartilage scales with the absorbed energy and time of irradiation. As can be seen in table 2.5, a higher thermal damage does inversely scale with the tensile strength, leading to the conclusion that a low irradiance and a short irradiation time – together with a well adapted solder (0.1 % ICG and 50 %BSA) – are suitable to achieve high tensile strengths and low thermal tissue damage.

2.7 Outlook

In future we plan to produce the matrices directly in the desired shape to prevent deformation of the matrices prior to the experimentation procedure. In a later stage these collagen matrices would allow doping of the implanted material with growth factors to stimulate growth and repair of the damaged cartilage in the joint, and/or to moderate the thermal damage induced to the cartilage. To overcome the problem of the diffusion of the solder into the matrices we would like to produce layered matrices with a absorbing membrane at the bottom connected to the collagen matrix on top which should lead to an more confined solder layer and therefore to a more homogeneous coagulation of this layer.

A feedback system to evaluate the exact endpoint of the soldering process needs to be incorporated into the experimental process. Up to now the endpoint of the irradiation has been visually evaluated. As soon as the scattering increased noticeably and the solder color changed from deep green to bright green the irradiation was stopped. This endpoint varies from solder to solder and for the different irradiances, leading to a variation in the achievable tensile strength. If the endpoint of the soldering process can unequivocally and consistently be determined the variation could be eliminated from the whole process.

To minimize the thermally induced tissue damage a circular irradiation of the solder – i.e. an irradiation of only the implant border – will be incorporated. This should lead to a considerably smaller thermal damage at the bottom of the defect; problems will arise through the smaller bonding area of the implant with the underlying cartilage.

If the reproducibility of the tensile strength measurements is more stable and the overall tensile strength values are higher, the soldering process needs

more evaluation in an in vivo application.

Chapter 3

Laser-assisted Ablation of Calcified Tissue

3.1 Introduction and Overview

3.1.1 Background

Aortic valve replacement is generally accomplished by a major surgical procedure, requiring general anaesthesia, opening of the ribcage, full cardiopulmonary[1] bypass with complete cessation of cardiopulmonary activity, recovery in an intensive care unit, five to ten days of hospitalization and 3 months of recuperation time [20].

The indications for aortic valve surgery are – among a variety of factors – relief of symptoms and/or the prevention of death or complications from the underlying disease. It is generally accepted that long-term results are better when a lesion is treated at an earlier stage.

Endovascular[2] procedures for valve replacement provide an alternative

[1] *Cardiopulmonary* – Relating to or involving both the heart and the lungs.
[2] *Endovascular* – Inside a blood vessel.

to conventional open heart surgery. Over the last few years a number of atherectomy[3] and endovascular devices used to remove plaque and other abnormal deposits from vessels have been developed which made minimally invasive techniques for replacing heart valves possible.

Although the devices and instruments used in these minimally invasive procedures are complex and hence relatively expensive, the procedures are gaining more and more acceptance, leading to a high demand in the clinical environment.

Percutaneous transluminal[4] procedures have substantial benefits both from the standpoint of health and safety as well as cost. Such endovascular procedures require a minimal invasion of the human body, which means a considerable reduction and sometimes even elimination of general anaesthesia and intensive care unit stay and therefore much shorter hospital stay [21,22].

Currently approximately 200000 defective heart valves are replaced annually, at an approximate cost of 12000 to 50000 Euro per procedure, thus it would be desirable if heart valves could be replaced using a minimally invasive technique. It would be especially advantageous if a defective heart valve could be removed using an endovascular procedure i.e. via the common femoral artery[5]. The whole procedure would then be carried out percutaneously and transluminally using the vascular system to convey an appropriate device to the aortic annulus to carry out the ablation procedure.

Two main problems arise with the replacement of calcified aortic heart valves inside the human body.

[3] *Atherectomy* – The surgical removal of arteriosclerotic plaque from the inner surface of a blood vessel.

[4] *percutaneous* – through the skin, *transluminal* – through a hollow space

[5] The A. femoralis communis is the artery leading from the groin to the heart.

- First the defective aortic valve has to be removed through an endovascular device, either as a whole or cut into small pieces. Therefore pieces smaller than the diameter of the instrument and blood vessel have to be generated.

- In a second step the new heart valve has to be positioned into the heart and fixed to the surrounding vessel. The implanted heart valve is in most cases an artificial replacement of the natural one, either a fully mechanical or porcine heart valve which has to meet the requirements for implantation through the chosen device.

3.1.2 Percutaneous Aortic Valve Ablation Using a Laser Device

In this study we only concentrate on the removal of calcified valves. The insertion of a novel collapsible heart valve using a new surgical procedure for minimally invasive implantation is investigated by another group [21]. The goal is to evaluate the feasibility of using an Erbium laser for the ablation of the calcified heart valve.

In the past, IR laser sources such as Erbium and Holmium (Er:YAG, 2.94 μm and Ho:YAG, 2.1 μm) have proven to be highly effective in cutting and drilling of biological tissue, either soft (like skin, tendons, etc.) or hard tissue (like bone).

The emphasis of this part of the research will be to examine the effects of these pulsed lasers on ablation of malfunctioning calcified aortic valves and to quantify this process. The best suited laser parameters (i.e. wavelength, pulse duration, pulse energy and repetition rate) for the proposed procedure have to be found aiming at a high cutting efficiency and at a maximum achievable

precision. The interest was focused on the evaluation of the relation between ablation efficiency and particle size of the ablation by-products and the laser parameters, namely pulse energy and repetition rate.

The problem to be solved is to design a device and method for the ablation of a human aortic valve during minimal invasive heart surgery in such a manner that the removal of the encrusted valve is executed rapidly, completely and in such a way that only a minimal secondary damage to the surrounding tissue is produced due to acoustical effects and heat propagation.

Through the ablation of the valves, debris is generated which is then freely moving in the blood circulation. To find a solution to avoid the generation of large scaled calcium debris is going to be very important. The hope is to find a method to collect the ablated calcium particles or the freely movable pieces of tissue and to completely extract them from circulation. These particles must be removed from the circulation, remaining in the patient they could lead to an occlusion of the smallest blood vessels which is potentially lethal, especially when the occlusion takes place in vessels supplying brain or lungs.

Besides the basic research a fiber delivery system transmitting the laser radiation from the laser system to the operation area will be developed and optimized capable to fit the clinical requirements:

- The system must in particular allow the aortic ablation during natural heart activity, thus avoiding cardiopulmonary bypass.
- The whole system needs to be small and flexible enough to fit inside an applicator which can be conveyed through the femoral artery to the heart of the patient.
- The system needs to withstand strain and torsion and must allow for sterilization to be suitable for a clinical in vivo application.

3.1.3 Photoablation of Biological Tissue

Er:YAG radiation at a wavelength of λ=2940 nm is strongly absorbed by water, which is present in abundance in all biological tissues. The optical penetration depth for light at this wavelength is only around 1 μm. To be able to ablate tissue with this laser, the radiation has to pass the aqueous media in which the heart valves are embedded during the cutting procedure (in vitro the calcified heart valves were embedded in saline solution). To achieve this, the fiber has to be moved in contact with the tissue to be ablated, or a transmitting water vapor channel between the distal fiber tip and the tissue needs to be generated which results in loss of pulse energy.

Through absorption in the tissue the temperature rises above 100 °C and the water inside the tissue instantly evaporates. Through the evaporation and through accompanying pressure effects, ablated tissue is explosively ejected from the laser generated cut. A goal of photoablative tissue processing is to achieve an ablation where the dimensions of the lateral and axial tissue damage induced through thermal and mechanical effects of the laser irradiation are small compared to the ablated tissue volume.

3.2 Material and Methods

3.2.1 Laser Source

A commercial Er:YAG laser (Fidelis Model 320A, Fotona, Slovenia) was used as a light source (λ=2940 nm), capable of emitting laser pulses with pulse energies between 40 mJ and 1 J in 10 mJ steps with a repetition rate of 2 to 50 Hz and a maximal average power of 15 W (see figure 3.1). The laser can be operated at various pulse lengths, emitting pulses ranging from 75 up to 950 ms. All experiments were performed at a pulse length of 250 ms.

Figure 3.1: Laser system

3.2.2 Light Delivery System

The cumbersome articulated mirror arm of the system was replaced by a fiber coupling device (see figure 3.2).

The laser light was coupled into a 325 μm (core diameter) sapphire fiber of 2 m length using an uncoated Calciumfluorite-lens ($CaFl_2$) with a focal length of 21 mm. The laser energy at the distal end of the fiber was measured by using an energy meter (Rj-7200 Energy Ratiometer, Laser Precision Corp, N.Y., USA).

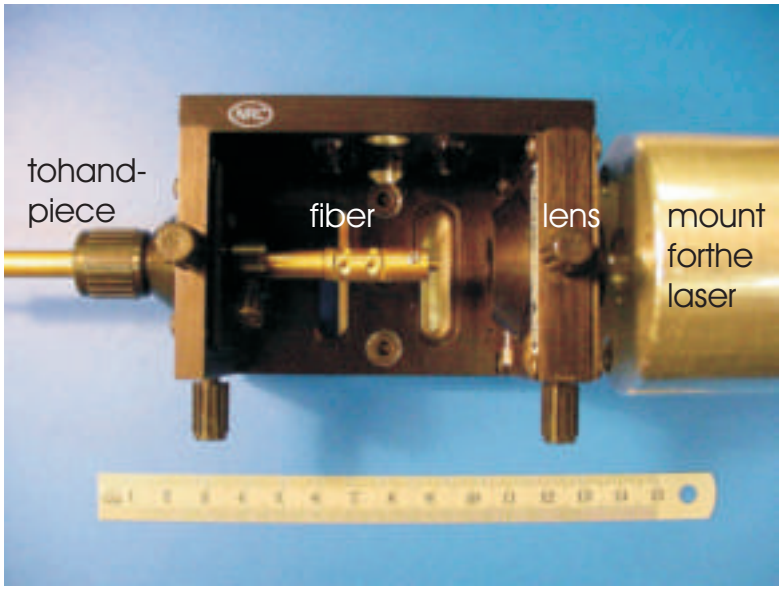

Figure 3.2: Fiber coupling device used to couple the emitted light from the laser into a 325 μm fiber instead of the mirror arm of the commercial system.

The maximum pulse energy obtained at the distal fiber tip was approximately 85 mJ at a repetition rate of 20 Hz.

The preliminary ablation experiments showed that the distance between the fiber tip and the tissue to be cut should be kept as small as possible to minimize loss of energy. The larger the distance between fiber tip and tissue surface, the more energy is consumed to establish a surgical delivery path

through the water [23]. Working in a non-contact mode although allowing a smooth movement of the fiber tip over the tissue surface involves a strong variation of the ablation depth since the fiber-tissue-distance cannot be kept perfectly constant with a hand guided fiber.

When the bare fiber was moved in contact with the rough tissue surface we observed a rubbing of the fiber on the surface preventing a smooth and constant movement of the tip. To prevent rubbing on the tissue surface a brass handpiece tip was designed (see figure 3.3), either 6 or 4 mm wide, which provided a much greater contact area to the calcified tissue, which consequently led to a smoother movement of the fiber on the tissue.

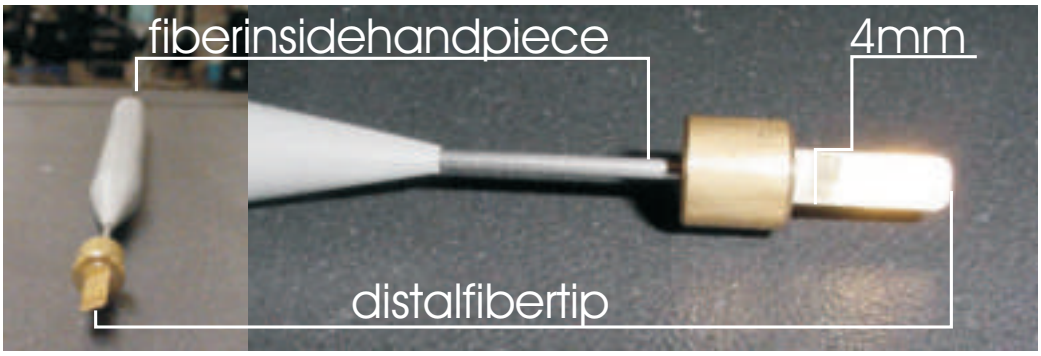

Figure 3.3: Handpiece and Handpiece detail

The thickness of the brass plate is only somewhat thicker than the fiber which allowed the movement of the fiber applicator inside the cut in the heart valve. We used this handpiece since it was already designed in the past for ENT (ear, nose and throat) and ophthalmologic applications and needed only minimal alteration (i.e. addition of the brass tip). This design of the handpiece is only the first step towards an endovascular fiber applicator to test the feasibility of using an Er:YAG laser for fast and precise ablation of calcified valves in an in vitro situation.

3.2.3 Heart Valve Samples and Ablation Process

Human calcified heart valves (obtained from the University hospital, Albert-Ludwigs-University of Freiburg, Germany) stored in formaldehyde (Formalin 4 %) after surgical extraction were used for our experiments. The laser cutting experiments were performed in a container filled with isotonic saline solution in which the valves were submerged and fixed with syringes. The ablation process was recorded with a CCD-camera for evaluation purposes. After cutting the samples were again put in formaldehyde for further standard histological examinations. In addition, the isotonic saline solution containing the ablation products was stored for quantification of particle size and distribution.

The ablation experiments were conducted at a laser repetition rate of either 20 or 30 Hz and an energy at the distal fiber tip between 30 and 85 mJ. The handpiece was hand guided and slowly moved in contact with the calcified tissue.

3.3 Results and Discussion

3.3.1 Laser and Laser Light Delivery System

The actual pulse energy differed compared to the settings on the display if the laser was running at high repetition rates. This effect was even noticed without the fiber, i.e. measured at the distal end of the mirror arm or at the outcoupling window of the laser system. For a low repetition rate, the maximum transmission through the fiber and in-coupling lens was about 40 % (see table 3.1).

f [Hz]	E [mJ]	E_{tip} [mJ]	T [%]
2	50	21	42
20	50	15	30
40	50	9	18

Table 3.1: Energy E_{tip} at the distal fiber tip depending on settings, f and E are the repetition rate and set pulse energy of the laser, respectively. T denotes the transmission through the whole system.

The typical transmission through a sapphire fiber at 2.9 μm is 60–70 % per meter [24, 25], resulting in a transmission of 36–50 % through a fiber of 2 m length. This explains the low transmission through the whole system at a low and moderate repetition rate. The low transmission at a higher repetition rate was mainly caused by fiber attenuation and heating of the fiber.

We assume that the sapphire fiber transmission decreases with increasing repetition rate and energy mostly due to heating of the fiber.

In addition the energy output of the laser varied $\pm$ 20 % compared to the set energy depending on the repetition rate. The details of one measurement can be seen in table 3.2.

An important factor in transmission through the whole system is the

f [Hz]	E [mJ]	Difference to 250 mJ [%]
2	305	+ 22
5	297	+ 19
10	281	+ 12
15	263	+ 5
20	235	– 6
30	203	– 19

Table 3.2: Energy E depending on repetition rate f of the system, The pulse energy of the laser system was set to be 250 mJ. The measurements were averaged over 100 pulses.

quality of the distal fiber end. Through the experimentation process, ablation products were deposited at the distal fiber tip, a process which decreases the output energy of the whole system during the cutting process.

To quantify the energy changes, the pulse energy was precisely measured before and after the ablation process.

3.3.2 Ablation

Figure 3.4 shows a snapshot of the valve and the distal fiber tip (valve number 6, see table 3.3). The brass end piece measures 4 mm, which allowed to produce an even smoother and a more accurate cut than with the 6 mm end piece.

Ablation experiments performed with the different pulse repetition rates and energies revealed that in view of particle size it is preferable to use low pulse energies together with a high repetition rate. By doing so, the size of the ablated particle is comparatively small. Nevertheless, some kind of filter must be put into the blood circulation if the ablation process is going to be performed in vivo.

To know the size of the ablation byproducts is important in view of designing a suited filter for filtering the particles out of the blood stream. If

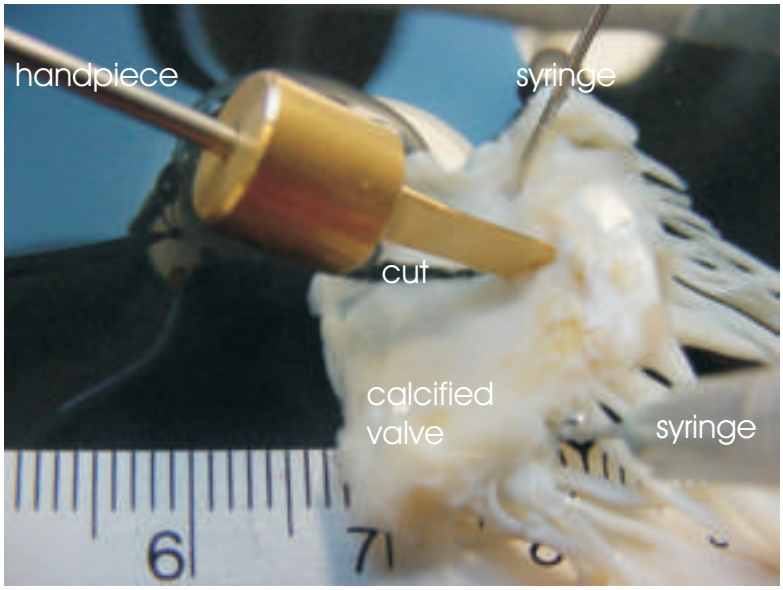

Figure 3.4: Heart valve and fiber tip during the experiment.

the particle size is much bigger than the size of the normal constituents of the blood (around 10 μm) then a filter will be much easier to implement, because it will not hinder the normal flow of the blood through the aorta.

As can be seen in table 3.3 cutting velocities of up to 15.3 mm per minute were achieved with an average of 7.67 $\pm$ 4.28 mm per minute. The ablation efficiency is high enough to provide a fast cut of the calcified heart valve. The cutting efficiency showed a great dependence on the rate of calcification of the tissue, heart valve number 5 and 11 were extremely calcified, leading to an uneven surface of the heart valve which made it difficult to correctly align the fiber tip on the tissue surface. As soon as the fiber loses contact to the tissue, the major part of the energy is lost into evaporation of the surrounding water and generation of a bubble channel.

The results suggest that the energy at the distal fiber tip is more important than the repetition rate in view of cutting efficiency.

Valve	f [Hz]	E_{tip} [mJ]	L [mm]	T [mm]	t [s]	v_2 [mm/min]
1	30	30	15	4	75	12.0
2	30	40	15	5	130	6.9
3	30	40	20	10	420	2.9
4	30	40	15	5	185	4.9
5	30	50	10		210	2.9
6	30	50	18	3	90	12.0
7	30	50	18	6	165	6.5
8	20	85	18	5	120	9.0
9	20	85	10	5	53	11.3
10	20	85	12	4	47	15.3
11	20	85	10	10	300	2.0
12	20	85	4	1	38	6.3

Table 3.3: Details of the experiments, f stands for the laser repetition rate, E_{fiber} denotes the energy measured at the distal fiber tip, L and T the length and thickness of the sample at the point of the cut, t denotes the cutting time and v_2 the cutting velocity. The thickness could not be recorded for sample 5, because the sample was extremely uneven and heavily calcified, leading to a variable thickness over the length of the cut.

3.3.3 Remnant Analysis

The remnants of the cutting procedure have been analyzed by a binocular (see figure 3.5) and a scanning electron microscope (SEM, see figure 3.6 and figure 3.7), which showed that the size of the debris ranges from smaller than 10 μm up to 1 mm.

The pictures have been analyzed using an Image-Examination Program (ImagePro) which is able to count and measure the single particles present in the pictures. To evaluate the distribution of the particle size, a histogram of the achieved data from the SEM-pictures at a magnification of 528 was obtained (see figures 3.7 and 3.8). Values resulting in a particle diameter smaller than 0.4 μm have been discarded, because particles of this size were only one pixel wide in the obtained images and could therefore not been clearly distinguished from noise artifacts in the images.

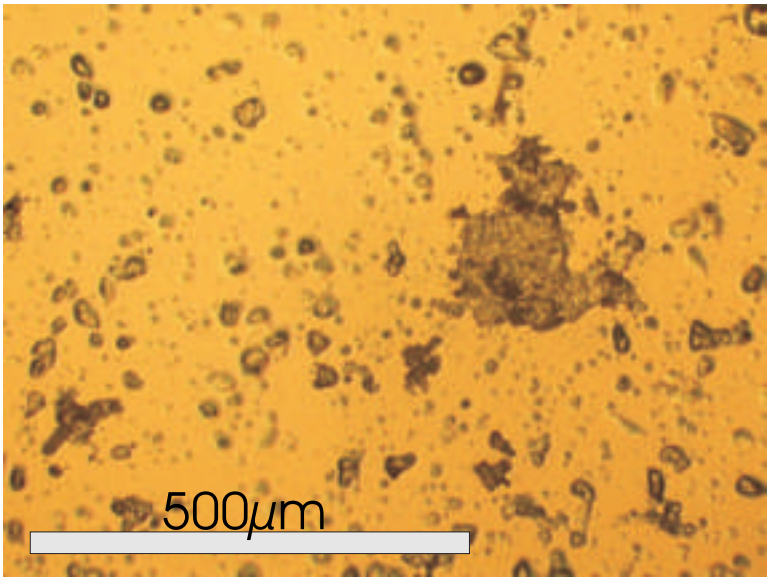

Figure 3.5: 10x magnified image of cutting remnants dried on a glass substrate.

A reason for not noticing any particles bigger than 30 μm is the choice of magnification and sector of the sample. As one can see in figure 3.5 there are remnants bigger than 200 μm in length. In figure 3.7(b) one can see a bigger particle on the right side. It's vertical size is 37 μm and the horizontal size is 17 μm. ImagePro is able to quantify the mean diameter of a particle, so this particle resulted in a value of approximately 27 μm.

3.3.4 Tissue Damage

The cut heart valves have been stained using the Masson trichrome staining method (MA) and the Haematoxylin/Eosin staining (HE) method, both standard histological staining methods. MA specifically stains the collagen whereas HE stains the whole tissue. HE and MA staining add the color up in the non-viable parts of the tissue, thus darker parts indicate dead tissue parts.

The tissue damage area can be seen as the dark colored area in the pic-

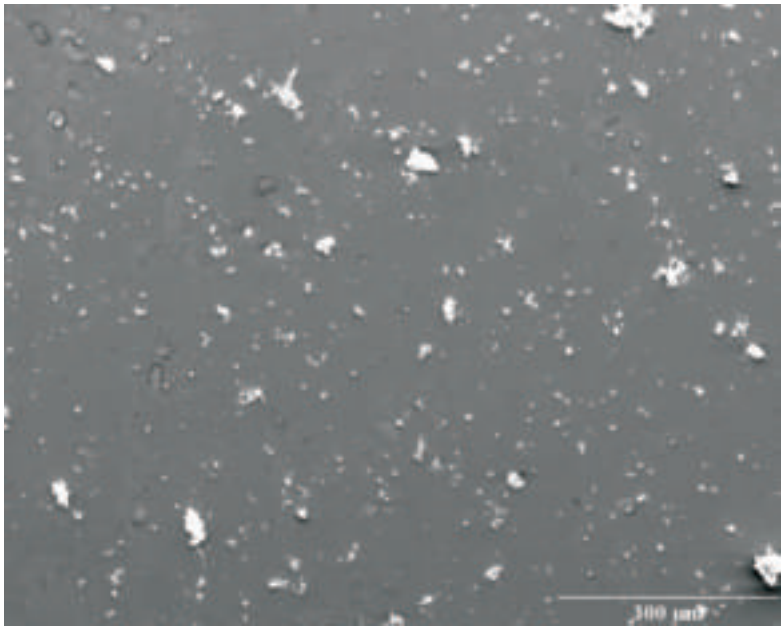

Figure 3.6: SEM picture of the cutting remnants, dried on a glass substrate, 100x magnification.

tures. As seen figure 3.9(c), the damage induced through laser cutting is not bigger than 15 μm.

A verification of the damaged area on all the pictures taken shows that the average damage is 12 $\pm$ 5 μm. The different staining methods show a slightly different damage area with HE indicating a greater tissue damage, which can be explained with the different sensitivities of the two methods.

The small thermally induced tissue damage should not impose complications, because the heart valve and the surrounding tissue are already heavily damaged through deposition of arteriosclerotic material.

This leads us to the conclusion that the main focus has to be put towards the development of a debris restraint system. This system must allow the execution of the laser ablation procedure in vivo. The size of the leftover particles may not exceed 8–10 μm which is the approximate size of a red blood cell, which is the greatest allowed diameter to pass through the human

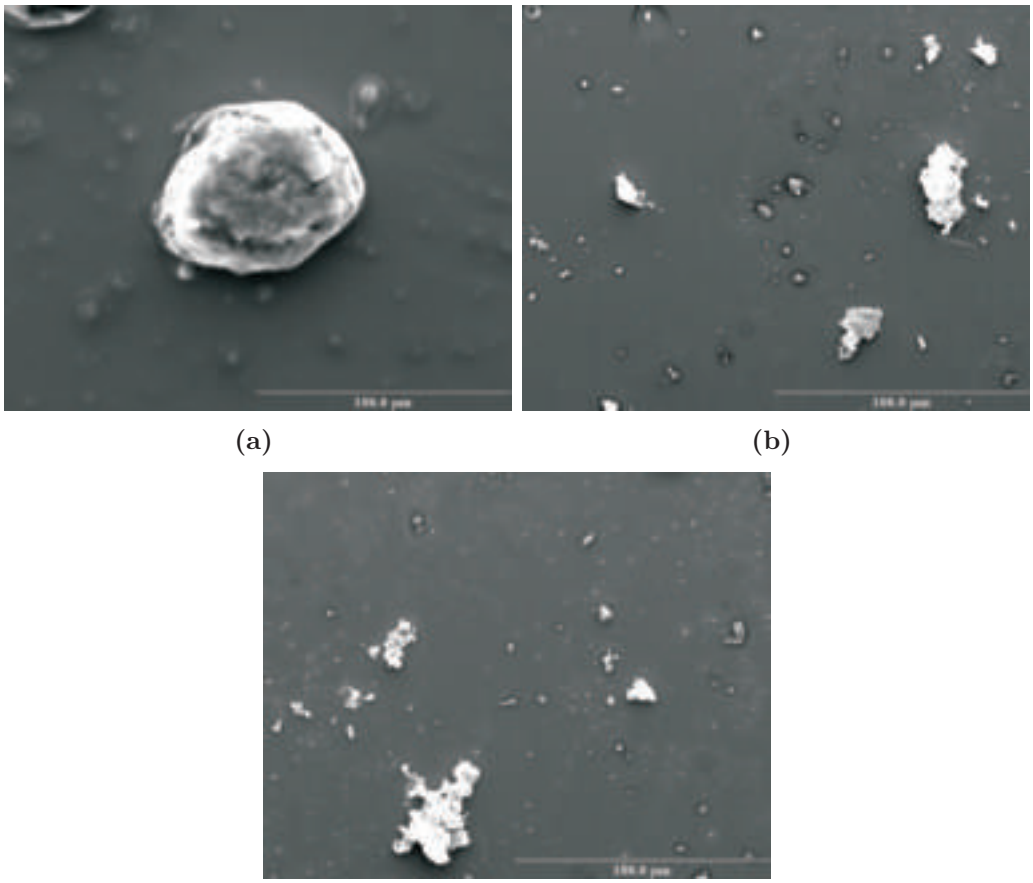

(a) **(b)**

(c)

Figure 3.7: SEM pictures of the cutting remnants, dried on a glass substrate, 528x magnification.

circulation system without imposing any harm[6]. Furthermore it should still be possible that the whole procedure can be carried out without the need of complete cessation of cardiopulmonary activity.

[6]Note that red blood cells can be deformed to help to pass through the smallest capillaries in the body.

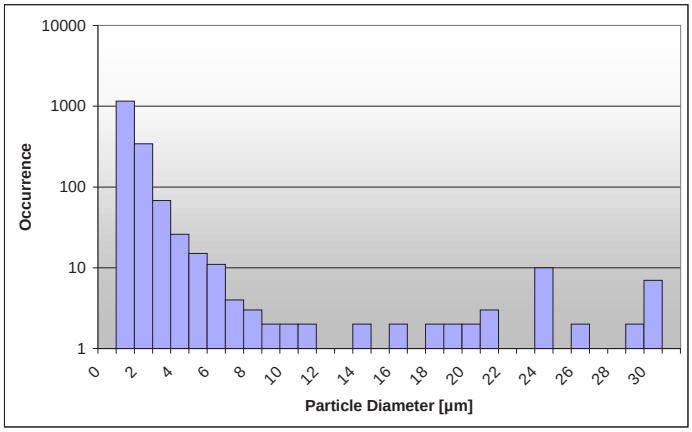

(a) Histogram over all the particles, logarithmic scale for Occurrence.

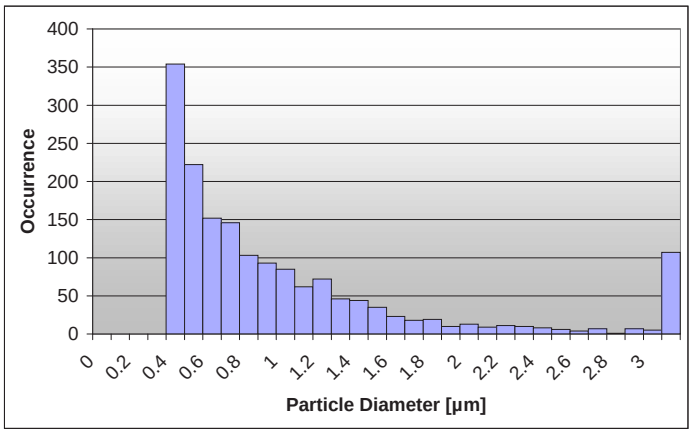

(b) Histogram over only the smaller particles.

Figure 3.8: Histogram of the particle size.

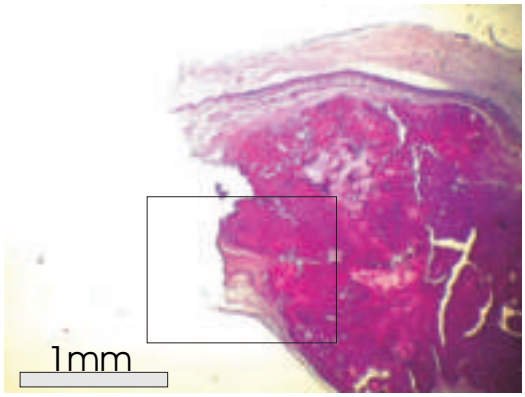

(a) 2.5x magnification

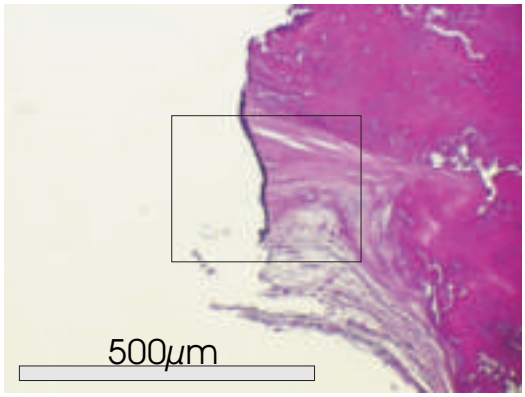

(b) 10x magnification

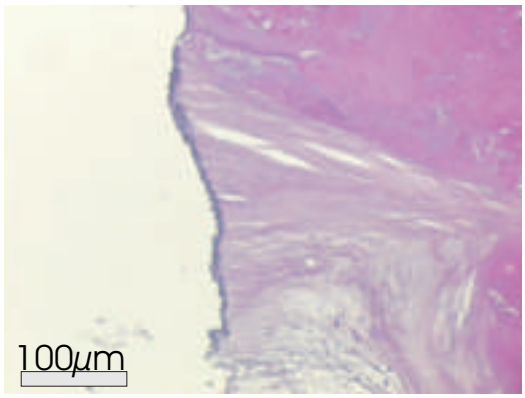

(c) 20x magnification

Figure 3.9: Histological examination (Haematoxylin/Eosin staining) at different magnifications, the black frame in the pictures marks the region of the next bigger magnification.

3.4 Conclusions

Calcified heart valves can be cut using an Er:YAG laser system. Nonetheless different difficulties arise, before this technique can be clinically applied:

- Development of an appropriate flexible fiber delivery system.
- Development of a guiding system capable to control the laser-tissue interaction area to prevent perforation of the vessel.
- All ablated particles have to be filtered out of the blood circulation.

Bibliography

[1] Beat Ott, Benno J. Züger, Dominique Erni, Andrej Banic, Thomas Schaffner, Heinz P. Weber, and Martin Frenz. Comparative in-vitro study of tissue welding using a 808 nm diode laser and a Ho:YAG laser. *Lasers Med Sci*, 16(4):260–66, 2001.

[2] K.M McNally, J.M Dawes, A.E. Parker, A. Lauto, J.A. Piper, and E.R. Owen. Laser-activated solid protein solder for nerve repair: In vitro studies of tensile strength and Solder/Tissue temperature. *Lasers Med Sci*, 14(3):228–37, 1999.

[3] B.J. Züger, Beat Ott, P. Mainil-Varlet, T. Schaffner, J.-F. Clemence, H.P. Weber, and M. Frenz. Laser solder welding of articular cartilage: Tensile strength and chondrocyte viability. *Lasers Surg Med*, 28(5):427–34, 2001.

[4] Benno J. Züger. *Reshaping and Welding of Cartilage with Lasers for Arthroscopic Applications*. PhD thesis, University of Bern, Switzerland, 2001.

[5] Kornel Köstli. *Pulsed Optoacoustic Spectroscopy and Imaging*. PhD thesis, University of Bern, Switzerland, 2001.

[6] J. M. Herrmann, C. Pitris, B. E. Bouma, S. A. Boppart, C. A. Jesser, D. L. Stamper, J. G. Fujimoto, and M. E. Brezinski. High resolution imaging of normal and osteoarthritic cartilage with optical coherence tomography. *J Rheumatol*, 26(3):627–35, 1999.

[7] U. Morgner, W Drexler, F. X. Kärtner, X. D. Li, C. Pitris, E. P. Ippen, and J. G. Fujimoto. Spectroscopic optical coherence tomography. *Optics Letters*, 25(2):111–13, 2000.

[8] Markolf H. Niemz. *Laser-Tissue Interaction: Fundamentals and Applications*. Springer-Verlag, Berlin, 1996.

[9] R.A. Stockwell. *Biology of Cartilage Cells*. Cambridge University Press, Cambridge, 1979.

[10] V.C Mow, A. Ratcliffe, and S.L.Y. Woo. *Biomechanics of Diarthoridal Joints*. Springer-Verlag, New York, 1990.

[11] L. Hangody, P. Feczko, L. Bartha, G. Bodo, and G. Kish. Mosaicplasty for the treatment of articular defects of the knee and ankle. *Clin Orthop*, 391(Suppl):328–36, 2001.

[12] D.K. Dew, L. Supik, C.R. Darrow 2nd, and G.F. Price. Tissue repair using lasers: A review. *Orthopedics*, 16(5):581–87, 1993.

[13] B. Alberts, D. Bray, A. Johnson, J. Lewis, M. Raff, K. Roberts, and P. Walter. *Lehrbuch der Molekularen Zellbiologie, 2., Korrigierte Auflage*. WILEY-VCH Verlag GmbH, Weinheim, Germany, 2001.

[14] K. L. Goa and P. Benfield. Hyaluronic acid. a review of its pharmacology and use as a surgical aid in ophthalmology, and its therapeutic potential in joint disease and wound healing. *Drugs*, 47(3):536–66, 1994.

[15] Daniel W. Ebert, Cynthia Roberts, Stuart K. Farrar, William M. Johnston, Alan S. Litsky, and Alicia L. Bertone. Articular cartilage optical properties in the spectral range 300-850nm. *J Biomed Opt*, 3(3):326–33, 1998.

[16] P. Mainil-Varlet, D. Monin, C. Weiler, S. Grogan, T. Schaffner, B. Züger, and M. Frenz. Quantification of laser-induced cartilage injury by confocal microscopy in an ex vivo model. *J Bone Joint Surg Am*, 83-A(4):566–77, 2001.

[17] Shawn Patrick Grogan, Balz Aklin, Martin Frenz, Thomas Brunner, Thomas Schaffner, and Pierre Mainil-Varlet. In vitro model for the study of necrosis and apoptosis in native cartilage. *J Pathol*, 198:5–13, 2002.

[18] J. F. Beek, P. Blokland, P. Posthumus, M. Aalders, J. W. Pickering, H. J. Sterenborg, and M. J. Van-Gemert. In vitro double-integrating-sphere optical properties of tissues between 630 and 1064 nm. *Phys Med Biol*, 42(11):2255–61, 1997.

[19] K. M. McNally, B. S. Sorg, E. K. Chan, A. J. Welch, J. M. Dawes, and E. R. Owen. Optimal parameters for laser tissue soldering. part I: Tensile strength and scanning electron microscopy analysis. *Lasers Surg Med*, 24(5):319–31, 1999.

[20] T. Ogata, T. Kaneko, T. Obayashi, S. Ishikawa, Y. Sato, N. Murai, N. Kaki, I. Shibasaki, K. Taniguchi, and Y. Morishita. Aortic valve replacement for aortic stenosis with a small mechanical prosthetic valve. *J Card Surg*, 17(1):70–74, 2001.

[21] Georg Lutter, Daniela Kuklinski, Georg Berg, Patrick Von-Samson, Juergen Martin, Michael Handke, Peter Uhrmeister, and Friedhelm Beyersdorf. Percutaneous aortic valve replacement: An experimental study. I. studies on implantation. *J Thorac Cardiovasc Surg*, 123(4):768–76, 2002.

[22] Younes Boudjemline and Philipp Bonhoeffer. Steps toward percutaneous aortic valve replacement. *Circulation*, 105(6):775–78, 2002.

[23] H. Pratisto, M. Ith, M. Frenz, and HP. Weber. Infrared multiwavelength laser system for establishing a surgical delivery path through water. *Appl Phys Lett*, 67:1963–65, 1995.

[24] Rick K. Nubling and James A. Harrington. Optical properties of single-crystal sapphire fibers. *Appl Optics*, 36(24):5934–40, 1997.

[25] J. J. Fitzgibbon, H. E. Bates, A. P. Pryshlak, and J. R. Dugan. Sapphire optical fibers for the delivery of erbium:YAG laser energy. *Biomedical Optoelectronic Instrumentation, SPIE*, 2396:60–70, 1995.

List of Figures

1.1 Scattering pattern of Rayleigh- and Mie-Scattering. 5

2.1 Fiber tip on sample during experiment. 13
2.2 Diagram of fiber and spot size on sample. 14
2.3 Zechner Drill with custom made retainer. 16
2.4 Cartilage sample with a piece of underlying bone. 17
2.5 Top and side view of a collagen matrix. 18
2.6 Jig used to cut the implants. 23
2.7 Preparation for tensile strength measurement. 25
2.8 Monte-Carlo-simulation. 28
2.9 Absorption and fluence simulations, gaussian beam profile. . . 30
2.10 Absorption and fluence simulations, tophat beam profile. . . . 31
2.11 Absorption and fluence simulations, tophat beam profile. . . . 32
2.12 Tensile strength as a function of ICG- and BSA-concentration. 34
2.13 Tensile strength as a function of BSA-concentration, 0.1 % ICG. 35
2.14 Irradiated cartilage defect with extremely shrunken matrix. . . 36
2.15 Live/Dead-Terminology 38
2.16 Live/Dead picture 39
2.17 Live/Dead picture 39
2.18 Live/Dead picture 43

3.1 Laser system 54
3.2 Fiber coupling device 55
3.3 Handpiece and Handpiece detail 56
3.4 Heart valve and fiber tip during the experiment. 60
3.5 10x magnified image of cutting remnants. 62
3.6 SEM pictures of the cutting remnants, 100x magnification. . . 63
3.7 SEM pictures of the cutting remnants, 528x magnification. . . 64
3.8 Histogram of the particle size. 65
3.9 Histological examination at different magnifications. 66

List of Tables

2.1 Collagen types. 19

2.2 Monte-Carlo-simulation parameters 28

2.3 Tensile strength depending on ICG- and BSA-concentration. . 33

2.4 Tensile strength depending on BSA-concentration, 0.1% ICG. 34

2.5 Details of thermal damage evaluation. 38

3.1 Energy at the distal fiber tip. 58

3.2 Energy depending on repetition rate 59

3.3 Details of the experiments. 61

Acknowledgements

My special thanks go to Prof. Dr. Martin Frenz, the head of the Biomedical Photonics Group, the former Laser Surgery Group, for his constant support. Not only in the laboratory, but also during the limited spare time we shared together I got to know him as a man with apparently unlimited knowledge in the field of Lasers and their use in Surgery and as a large-hearted person. I have to apologize to Martin that he had to cope with my urge to write this thesis using LaTeX.

I thank Prof. Dr. Heinz P. Weber for giving me the opportunity to start this master thesis in the Laser Department at the Institute of applied physics in Bern and to finish it in the Biomedical Photonics Department.

Another special thanks go to the colleagues in our group; Benno Züger, which introduced me here, Beat Ott, which was a great help in the lab, and all the other people still present in the Biomedical Photonics Group.

I happily shared my office with Res Friedrich, the technician of our group which is amazingly helpful and had great ideas as how to construct objects for my needs. Vreni Winkelmann was extremely helpful with the preparation of the Live/Dead Staining assays and histological tissue samples. Simona Berardi from Centerpulse was a great help with the preparation of the solders and a competent contact concerning the chemical side of this thesis. The SEM-images could not have been done without Eva Krähenbühl.

During my diploma studies my fellow students, especially Christian Sigrist, Beat Deuber, Urs Rohner and Oliver Nyffenegger, were very helpful. They helped me to focus on other things than Laser Surgery and to cope with the quirks of managing to work with LaTeX on a Windows-Machine. Thanks for being here at the University. Bidu, thanks for reading my thesis and for pointing out some errors. Sigi, we need to practise our DDC-Skills if we want to score big time in three weeks!

I'd also like to thank my friend Peter Bezak, and my friends and flatmates Wolf Röcken and Marcel Rolli for being here. We share great times outside the academic tuft.

I thank my parents Daniel and Heidi Haberthür for the immense support they granted me throughout all the past years. I would not be here without you! My sister Nina Haberthür is the bestest sister i could ever have had, I love you all.

Finally I would like to thank Nina Hostettler for being my princess and for coping with me in the last weeks. I love you!

Bern, 30th August 2002.